Facies (2024) 70:16
https://doi.org/10.1007/s10347-024-00690-1

ORIGINAL ARTICLE

# Controls on mesophotic carbonate facies and sediment distribution across the Maltese shelf, central Mediterranean Sea

Or M. Bialik[1,2,3] · Giovanni Coletti[4] · Christian Berndt[5] · Mark Schmidt[5] · Aaron Micallef[6]

Received: 17 July 2024 / Accepted: 13 September 2024
© The Author(s) 2024

## Abstract

Although ~ 20% of global carbonate production occurs on extra-tropical carbonate depositional systems, our understanding of these environments still lags behind that of tropical ones. The Maltese shelf in the central Mediterranean offers an opportunity to study in situ facies distribution and the factors controlling it in a light-dominated setting. The investigated region of the Maltese shelf visually exhibits three main depositional environments: seagrass meadows, sand flats and rhodolith and maerl beds. While visually distinctive, the grain composition of the sediments does not provide a clear differentiation of the three environments but rather a gradient. This gradient is marked by increasing grain size with water depth, a transition from green to red calcareous algae and an increase in the fraction of low magnesium calcite of total carboantes. While some of these features can be explained by changes in light availability, other factors are also in play. Baffling by seafloor vegetation and currents, storms and internal waves inducing sediment reworking appear to play important roles in governing the sediment texture and composition across the Maltese shelf. The role of seagrass meadows in regulating production and accumulation rates of carbonates appears to be of greater importance in Mediterranean C-type carbonate factories than in southern Atlantic ones and this could be an important marker to identify them in the geological record.

**Keywords** Coralline algae · Maerl · Calcareous sand · Carbonate factories · Malta

## Introduction

Carbonate factories represent both the locations of carbonate production and the associations of various carbonate-producing organisms (Tucker and Wright 1990; Schlager 2003). Given the fossilization potential of carbonate-producing organisms, these factories have a massive fossil record spanning most of Phanerozoic, providing a powerful archive for investigating the evolution or our planet (Kiessling et al. 1999, 2002; Halfar and Mutti 2005; Bosellini and Perrin 2008; Westphal et al. 2010; Perrin and Bosellini 2012; Pomar et al. 2017; Mariani et al. 2022; Bialik et al. 2023). The two most common shallow-water carbonate factories in modern oceans are the T-Type and C-Type factories (Schlager 2005; Michel et al. 2019; Reijmer 2021). T-Type factories (T stands for tropical or "top-of-the-water-column") are the main ones associated with modern flat-topped platforms (sensu, Williams et al. 2011). They develop in tropical settings where light is mostly available and today they are usually dominated by zooxanthellate corals and calcareous green algae. C-Type factories (C stands for cool-water or controlled precipitation) span much larger depth and

✉ Or M. Bialik
obialik@ocean.org.il

✉ Giovanni Coletti
giovanni.coletti@unimib.it

1 Institute of Geology and Palaeontology, University of Münster, Corrensstr. 24, 48149 Münster, Germany

2 Department of Marine Geosciences, The Leon H. Charney School of Marine Sciences, University of Haifa, 31905 Carmel, Israel

3 Israel Oceanographic and Limnological Research, National Institute of Oceanography, 310800 Haifa, Israel

4 Department of Earth and Environmental Sciences, University of Milano-Bicocca, Piazza Della Scienza 4, 20126 Milan, Italy

5 GEOMAR Helmholtz Centre for Ocean Research Kiel, Wischhofstraße 1-3, 24148 Kiel, Germany

6 Monterey Bay Aquarium Research Institute, Moss Landing 7700, CA, USA

Published online: 30 September 2024

temperature ranges and are usually dominated by bryozoans, molluscs and coralline algae. Many studies have addressed the depositional environment of C-Type factories (Bosence and Pedley 1982; Basso 1998; Nebelsick and Bassi 2000; Rasser 2000; James et al. 2001; Nalin et al. 2006; Bassi and Nebelsick 2010; De MacEdo Dias and Villaa 2012; Halfar et al. 2012; Braga et al. 2012; Gaglianone et al. 2017; Coletti and Basso 2020; Coletti et al. 2022), but most of these studies have examined geological deposits, with only a small fraction of researchers focusing on ground truthing modern systems. This stands in stark contrast to T-Type factories, where modern examples and their facies distribution have been extensively investigated (Alongi 1989; Smith et al. 1998; Gischler 2006; Gischler et al. 2008; Bergman et al. 2010; Harris et al. 2015). Among C-Type factories there is also a disparity between the nutrient-limited carbonate factory (n/C-Type), present on most oceanic margins, and the light-limited carbonate factory (l/C-Type), which is almost exclusive to the Mediterranean Sea (Sciberras et al. 2009; Martin and Gattuso 2009; Michel et al. 2019; Rindi et al. 2019; Laugié et al. 2019; Guy-Haim et al. 2020; Reijmer 2021).

Works done on n/C-Type carbonate factories in South Australia and in the western Atlantic (James et al. 2001; De MacEdo Dias and Villaa 2012; Halfar et al. 2012) show a significant grain size and compositional variability related to hydrodynamic energy and nutrient availability. Much less is known, in this regard, about the l/C-type factories of the Mediterranean Sea (Fichaut et al. 2003). Our understanding of the spatial distribution of the l/C-Type carbonate factory also remains poor. Detailed geophysical studies of l/C-Type systems such as the Maltese shelf (Micallef et al. 2012; Foglini et al. 2016) suggest that a combination of depth and seafloor morphology controls the distribution of sedimentary facies by influencing the local movement of water masses and, consequently, temperature profiles and light availability. Another relevant and poorly constrained element governing C-type factories is reworking. Since these factories usually lack a marginal rim, there is no physical barrier preventing movement of sediment, and many C-type factories end up developing geometries similar to those of siliciclastic depositional systems (Schlager 2005; Pedley and Carannante 2006; Pomar et al. 2017). Furthermore, the differences between the diagenetic pathways of aragonite, which prevail in T-type factories, and that of high magnesium calcite (HMC) that prevails in the C-type factories result in the presence of more loose material in C-type systems. These loose grains are redistributed by currents and waves, as well as by metazoans such as fish and echinoderms. As a result of that, grain (allochems sensu Folk 1959) assemblages in C-type systems will display a complex composite signal comprised of a "productivity" signal and a "reworking" signal (Pomar and Kendall 2008).

While major uncertainties on the dynamics of modern carbonate depositional systems dominated by C/type factories (and by l/C-type in particular) still exist, the benthic communities of these factories are currently exposed to multiple stressors, ranging from the large-scale effects of global warming and ocean acidification (Martin and Gattuso 2009) to local activities such as fishing and trawling (Sciberras et al. 2009). Although recent studies have undoubtedly proved the sensitivity of these carbonate producers (e.g., Guy-Haim et al. 2020), most of them are still poorly understood and their distribution is mostly unknown (Rindi et al. 2019). As such, understanding the environment of modern C/type factories and establishing a good sedimentological basis for their exploration is crucial.

The Maltese shelf, previously investigated by multiple studies (Lanfranco et al. 1999; Sciberras et al. 2009; Micallef et al. 2016; Prampolini et al. 2018; Ferraro et al. 2020; Gatt 2021; Bialik et al. 2022) offers a good setting to improve our understanding of l/C-type carbonate system. In order to expand the existing knowledge of non-tropical grain assemblages, their composition, sedimentological characteristics and palaeoenvironmental significance have been examined in this project. This study aims at ground-truthing prior geophysical studies on the Maltese shelf, delineating the sedimentary facies and their distribution. Sediment samples have been collected and analysed, providing quantitative data on their sedimentological and mineralogical characteristics and on the abundance of the main carbonate producers. These data are then related to abiotic parameters to better highlight the underlying controls.

## Geological setting

The Maltese shelf is a shallow water plateau in the central Mediterranean Sea (Fig. 1A), surrounding the Maltese archipelago. It is an elevated feature elongated along an NW–SE trend. It is located in the north-eastern part of the Pelagian Block, the remnant of an ancient carbonate platform initially formed in the Tethys Ocean during the Palaeogene (Jongsma et al. 1985; Bishop 1988; Micallef et al. 2016). As of the Late Miocene, the area experienced uplift driven by a SE-NW directed horizontal shortening as plate convergence between Africa and Europe changed the regional tectonic stress field (Reuther et al. 1993; Adam et al. 2000; Gutscher et al. 2016). Late Pleistocene sedimentation in the region is considered to be mostly aggradational (Osler and Algan 1999), with the sediment covering the shelf being predominantly sand to gravel-sized biogenic grains (Micallef et al. 2012). This material is mostly generated on the shelf with a limited supply of detrital material from the archipelago (Gatt 2021).

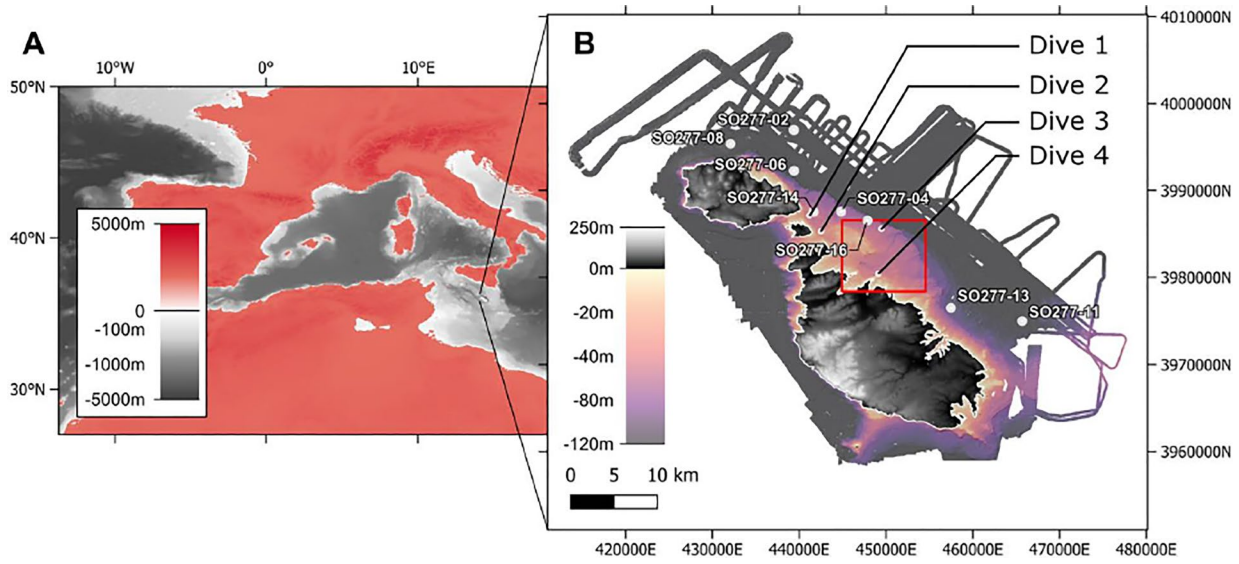


**Fig. 1** **A** Location map showing the position of the Maltese Archipelago relative to the rest of the Mediterranean. **B** Blowup shows the bathymetry for the Maltese shelf and location of the study area (red frame). All maps are north-oriented

The shelf ranges in depth between 0 and 100 m below the present sea level (mbsl) and terminates with a steep margin, resulting in a 10 m to 30 m escarpment. This slope is steeper in the NE and more gradual to the SW. The majority of the shelf is exposed only to the uppermost part of the water column comprising the local surface water and the Atlantic Waters (Warn-Varnas et al. 1999; Ben Ismail et al. 2012; Placenti et al. 2013). Oceanographic studies in nearby southern Sicily indicate that surface waves in the region exhibit primarily an E-W main direction with their maximum energy at around 25 mbsl (Iuppa et al. 2015). As there is no available Maltese data at this time and given the small distance, we assume similar behaviour in Malta as well. The regional climate is warm and arid (Galdies 2011) with low to medium wind intensity. Despite that, rare but extremely powerful storm events are known in the region, transporting massive boulders along the shore and enhancing local coastal erosion (Grabowska 2010; Biolchi et al. 2016; Causon Deguara and Gauci 2017).

## Methods

### Study site

The area selected for this study is a sector of the Maltese shelf located northeast of Mellieħa (Għadira) Bay (Fig. 1B). This area was selected based on the extensive availability of data for planning sampling activities and for the wide range of seafloor types. Primary data collection for this study was carried out in two parts. Seafloor imaging and oceanographic data were collected during RV Sonne expedition SO277 (Berndt et al. 2021), in which several of the coauthors participated. Surface sediments were collected during a subsequent dedicated sampling campaign.

### Seismic reflection profile

A multichannel seismic reflection profile (P2000_2115_2857), crossing the shelf in the study area, obtained by RV Sonne expedition SO277 (Berndt et al. 2021), was taken into consideration for the analysis. The acquisition was carried out with a 187.5 m-long 120-channel Geometrics GeoEel streamer and two GI-Guns (Generator-Injector Guns) as a seismic source. The data used in the current research were then processed with SeismicUnix and Omega at GEOMAR. This processing included FX-time migration with a constant velocity of 1500 m/s. The data were then visualized and interpreted using the IHS Markit Kingdom software at the University of Malta.

### Water column parameters

Abiotic parameters of the water mass were collected as part of R/V Sonne expedition SO277 (Berndt et al. 2021). These include CTD data (Supplement 2) collected on the shelf with an attached camera (see Fig. 1B for locations). For the current research these temperature and salinity data from the CTD casts were binned to 10 s intervals and were used to calculate water density in accordance to the UNESCO formulation (UNESCO 1981).

The Brunt–Väisälä frequency (N) distribution in the water column (indicating the potential capacity to propagate internal waves) was calculated using Eq. 1 (Vallis 2017):

$$N = \sqrt{\frac{-g}{\rho}\frac{d\rho}{dz}} \quad (1)$$

where ρ is the potential density of the fluid, g is the local acceleration of gravity and z is water depth.

Data for station SO277-02 are shown in Fig. 2, data from all other stations processed are included in supplementary material (10.6084/m9.figshare.20330490). Wave data were taken from the Mazara del Vallo station offshore Sicily and then reprocessed (Fig. 3).

## Seafloor imagery

The video data from the CTD casts were integrated using Agisoft to generate photomosaics. Image quality was too low to use this information for more than general context. Higher resolution imagery with better spatial coverage was collected by autonomous underwater vehicle (AUV) dives using Girona 500 AUV (IQUA Robotics, Girona, Spain) equipped with a CoraMo mkII Camera which can take up to 2 images per second with a resolution of 12.34MP. Operation and imaging followed Linke et al. (2015). The imagery collected during these dives was similarly integrated into mosaics. These mosaics were analyzed in the

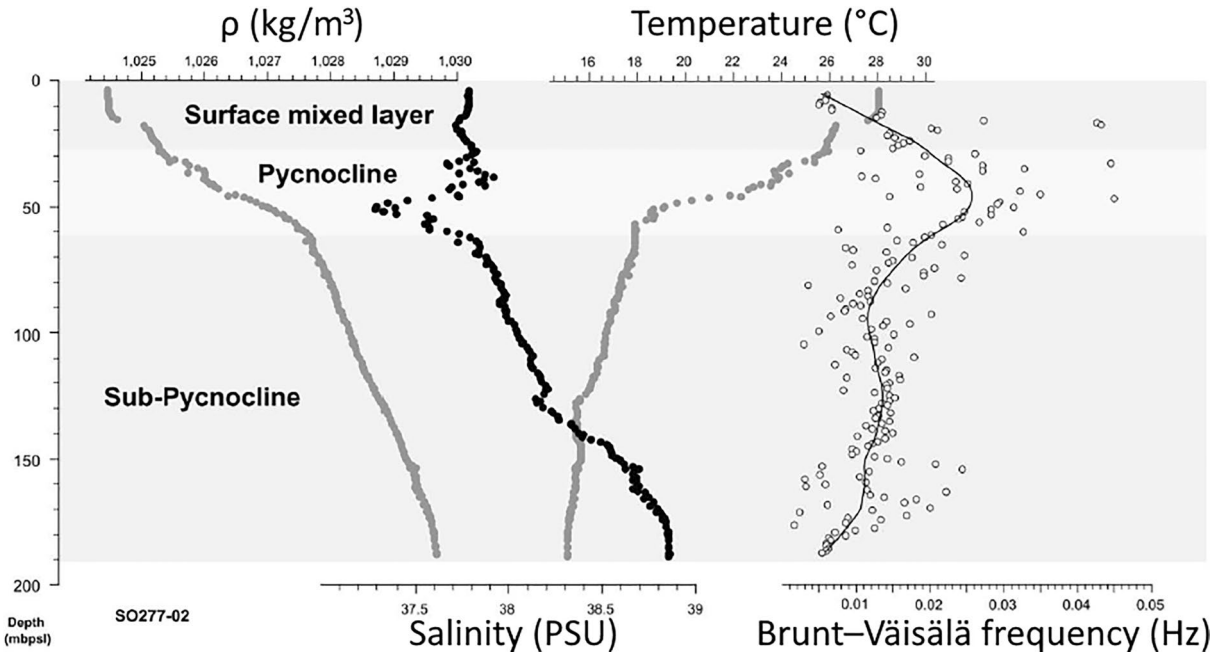


**Fig. 2** Representative profile of density (ρ), salinity, temperature and Brunt–Väisälä frequencies for the region from CTD station SO277-02

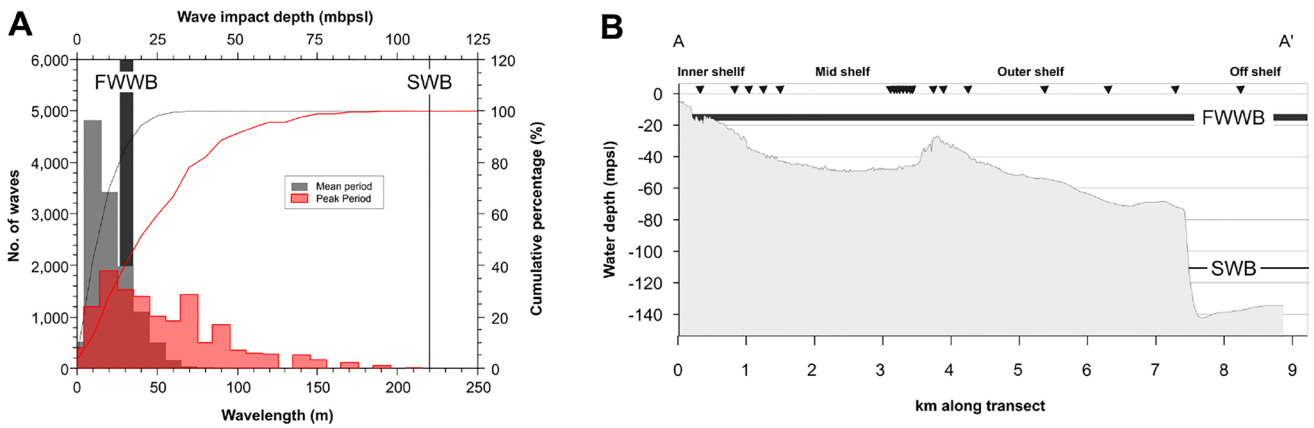


**Fig. 3** **A** Wavelength distribution in the Sicily Channel and inferred FWWB and SWB; **B** Profile of the Maltese shelf in the study area (see Fig. 2A) with the depths of the FWWB and SWB

context of the backscatter-based classification to identify the seafloor variability within the sampling error of the sampling tools. Mosaics were imported into QGIS (Sutton et al. 2021) and geolocated relative to seafloor features. Each mosaic was visually inspected to identify the seafloor elements which were mapped into main elements. Detailed description and analysis of the AUV data are provided in Supplement 1, with a summary and key notes provided in the results.

## Sample acquisition and processing

A sampling survey was planned using the bathymetric and backscatter data previously described and analyzed (Micallef et al. 2012, 2013; Foglini et al. 2016; Prampolini et al. 2017, 2018; Berndt et al. 2021). The depth range in the study area where sampling was permitted (defined in coordination and under permit with the Maltese authorities), extends from 10 to 140 mbsl (Fig. 4A). Sample positions were selected to cover the full depth range of the

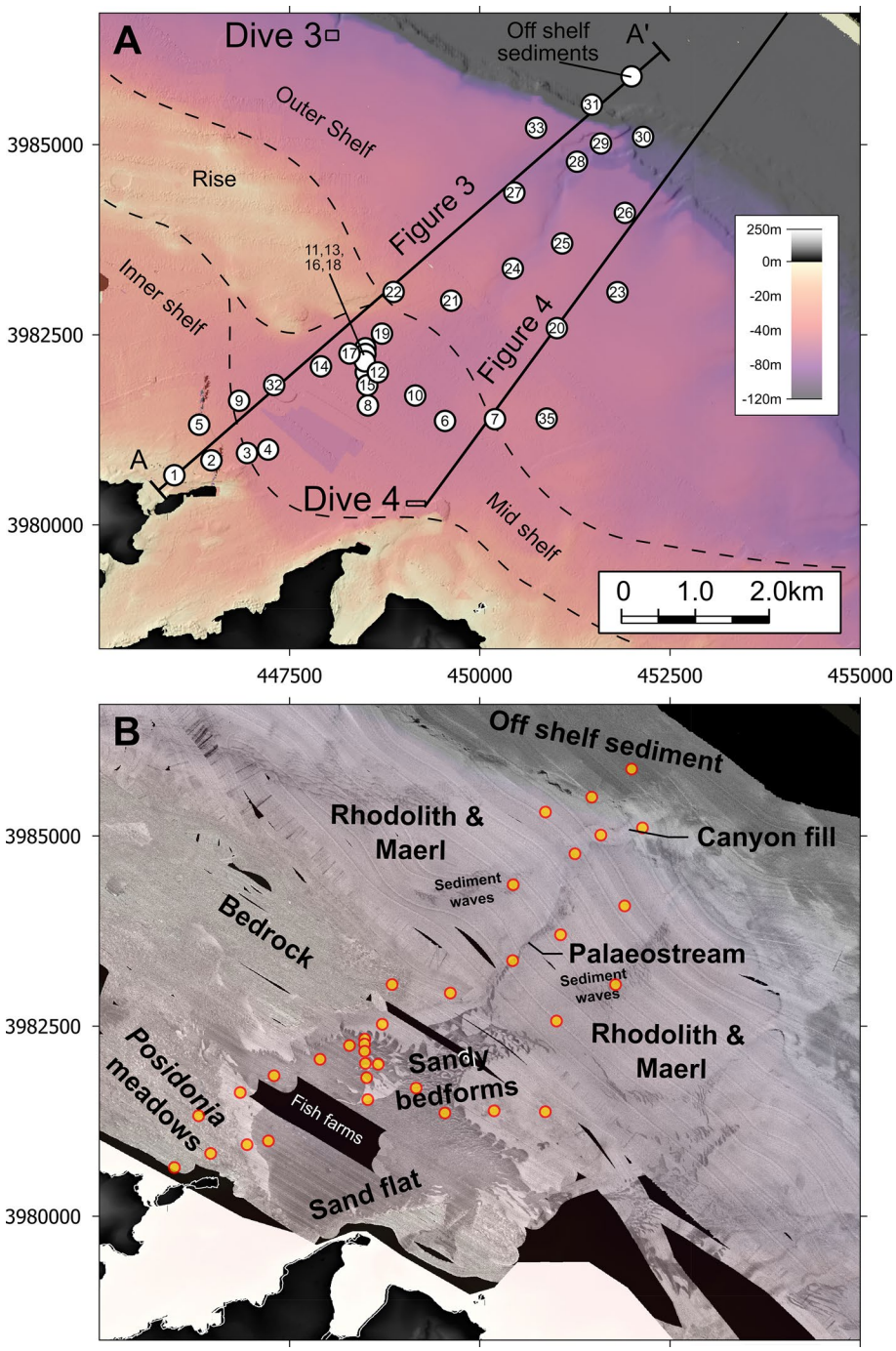


**Fig. 4** **A** Bathymetry of the study area showing the locations of the grab samples collected in this study, lines indicate the position of the seafloor profile shown in Fig. 3 and seismic profile shown in Fig. 3. Differentiation of the inner, mid and outer shelves here is based on physical features separating the different zones. **B** Multibeam backscatter of the study area showing the different bathymetric domains as mapped by prior studies (Micallef et al. 2012; Foglini et al. 2016; Prampolini et al. 2017, 2018; Berndt et al. 2021). All maps are north-oriented

shelf and all of the major seafloor facies and geomorphological elements of the seafloor identified in Micallef et al. (2012), including (from SW to NE): seagrass (*Posidonia*) meadows; sand flats; exposed bedrock; ranges of sandy bedforms; rhodolith and maerl beds; patches of sediment waves; a palaeochannel which opens to a canyon (sediment filled) and off-shelf sediments (Fig. 4B), the terminology follows previously established ones synthesized from previous studies on the region (Micallef et al. 2012, 2013; Prampolini et al. 2017). These seafloor classes were ground-truthed by ROV dives. Given the existing uncertainties in placing the boundaries between the various parts of the shelf solely on hydrodynamic energy (Lentz and Fewings 2012; Garvine 2021and references therein), the subdivision of the shelf into the inner, middle and outer shelves follows Micallef et al. (2013) and is primarily based on geomorphological features and the distance from the shoreline.

Sampling was carried out at the end of August 2021 aboard the service vessel Gold Finder using an Evenco (Auckland, New Zealand) Shipek grab with a 3000 mL scoop volume. The estimated error on location for each station is ~ 20 m (Fig. 4A, Table 1). Samples were transferred from the grab to plastic bags onboard. With return to the port an aliquot of each sample was washed with fresh water over a 63 µm mesh. Both the washed and unwashed splits were allowed to air dry until fully dry before any further step was undertaken.

**Table 1** Location table for all grab samples taken for this study. See Supplement 3 for more information

| New label | Long | Lat | Water depth (mpsl) | Distance from shore (m) | Texture (Dunham) | Domain |
|---|---|---|---|---|---|---|
| 1 | 14.40064 | 35.96877 | – 15 | 409 | | Rocks and Reefs |
| 2 | 14.40631 | 35.97061 | – 28 | 659 | Poorly washed grainstone | Seagrass meadows |
| 5 | 14.40434 | 35.97497 | – 36 | 1033 | Poorly washed grainstone | Seagrass meadows |
| 3 | 14.41138 | 35.97171 | – 45 | 1156 | Poorly washed grainstone | Mearl |
| 4 | 14.41432 | 35.97205 | – 45 | 1456 | Grainstone | Calcareous sand |
| 9 | 14.41021 | 35.97789 | – 44 | 1576 | Bafflestone | Mearl |
| 32 | 14.41538 | 35.97973 | – 48 | 2087 | Grainstone | Calcareous sand |
| 7 | 14.4474 | 35.97576 | – 48 | 2509 | Floatstone | Mearl |
| 6 | 14.44029 | 35.97556 | – 54 | 2553 | Floatstone | Sand waves |
| 35 | 14.45492 | 35.97587 | – 48 | 2714 | Grainstone | Mearl |
| 14 | 14.42207 | 35.98199 | – 50 | 2799 | Poorly washed grainstone | Sand waves |
| 10 | 14.4358 | 35.97859 | – 53 | 3028 | Poorly washed grainstone | Sand waves |
| 8 | 14.42911 | 35.97724 | – 52 | 3190 | Grainstone | Sand waves |
| 17 | 14.42632 | 35.98358 | – 50 | 3279 | Grainstone | Calcareous sand |
| 11 | 14.42898 | 35.9808 | – 51 | 3356 | Floatstone/Rudstone | Sand waves |
| 13 | 14.42883 | 35.9814 | – 51 | 3375 | Grainstone | Sand waves |
| 15 | 14.42861 | 35.98236 | – 51 | 3410 | Poorly washed grainstone | Sand waves |
| 16 | 14.42853 | 35.98309 | – 52 | 3448 | Grainstone | Sand waves |
| 18 | 14.42866 | 35.98407 | – 51 | 3522 | Grainstone | Sand waves |
| 12 | 14.43051 | 35.98123 | – 52 | 3528 | Poorly washed grainstone | Sand waves |
| 19 | 14.43098 | 35.98584 | – 49 | 3846 | Rudstone | Mearl |
| 20 | 14.45667 | 35.98662 | – 55 | 3905 | Grainstone / Floatstone | Mearl |
| 21 | 14.4409 | 35.98984 | – 48 | 4106 | Rudstone | Mearl |
| 22 | 14.43267 | 35.99088 | – 37 | 4338 | Grainstone / Floatstone | Seagrass meadows |
| 24 | 14.45002 | 35.9936 | – 60 | 4514 | Rudstone | Mearl |
| 23 | 14.46541 | 35.99093 | – 60 | 4728 | Rudstone | Mearl |
| 25 | 14.45711 | 35.99685 | – 59 | 5013 | Grainstone / Floatstone | Mearl |
| 27 | 14.45009 | 36.00271 | – 66 | 5524 | Poorly washed grainstone | Mearl |
| 33 | 14.45343 | 36.00727 | – 73 | 5621 | Floatstone | Mearl |
| 26 | 14.46623 | 36.00028 | – 69 | 5707 | Rudstone | Mearl |
| 28 | 14.45918 | 36.00627 | – 83 | 6086 | Poorly washed grainstone | Mearl |
| 29 | 14.46262 | 36.00852 | – 74 | 6429 | Grainstone | Mearl |
| 30 | 14.46881 | 36.00937 | – 105 | 6751 | Rudstone | Mearl |
| 31 | 14.46171 | 36.01298 | – 141 | 6879 | Packstone | Mearl |

Fully dried samples were photographed and initially described by visual observation. Following that, a description of size and components was carried out under the stereomicroscope (Supplements 3, 4). The main components present in each sample were firstly evaluated in a semi-quantitative fashion (D – Dominant, only component in most field of views; A – Abundant, present in large amounts in each field of view; C – Common, present in any field of view; F – Few, present in some fields of view; P – Present, only individual specimen found in all fields of view surveyed). The texture of every sample was also named in accordance to the modified Dunham classification (Dunham 1962; Embry and Klovan 1971; Lokier and Al Junaibi 2016) commonly used for textural description of modern calcareous sediment (Gischler 2006; Reijmer et al. 2009; Betzler et al. 2015; Reolid et al. 2024). Since grain-size ranges extended into the gravel size, grain-size analysis was done optically. Multiple fields of view of each sample were collected and individual grain sizes were measured using the ImageJ software (Rasband and Contributors 2021). At least 500 measurements (or all grains present) were collected for each sample. Mineralogical determination was carried out using X-ray diffraction (XRD) on bulk powdered samples. Analysis was carried out using a Rigaku MiniFlex 600 benchtop X-ray diffractometer (30 kV/10 mA from 3° to 70° at 0.05° increments by point detector) with a Cu target X-ray source. The relative abundance of carbonate species was estimated using the relative intensity ratio methods (Hubbard and Snyder 1988).

Following this phase, thin sections were prepared from unwashed, un-sieved samples representative of the variability initially assessed using preliminary visual estimation. These samples were processed according to standard procedures (Flügel 2010). Quantitative evaluation of constituents was carried out using point counting (Supplement 5) with detailed component descriptions. Statistical analysis of the grain assemblages was carried out following the approach and method outlined in Bialik et al. (2021) using PAST (Hammer and Harper 2007). All values for both preliminary visual analysis and detailed thin-sections analysis are freely available and accessible at https://doi.org/10.6084/m9.figshare.20330490.v3.

## Results

### Seismic reflection profile

The recent sedimentary cover over most of the Maltese shelf is a few metres thick in most places, although there are sediment-filled pockets. The thickest of those appears to be the intrashelf basin in the southwest of the study area (Fig. 4), hosting ~ 20 m of sediment fill (Fig. 5). In the off-shelf area a more significant sediment accumulation is found, exceeding 30 m above the acoustic basement (Fig. 5).

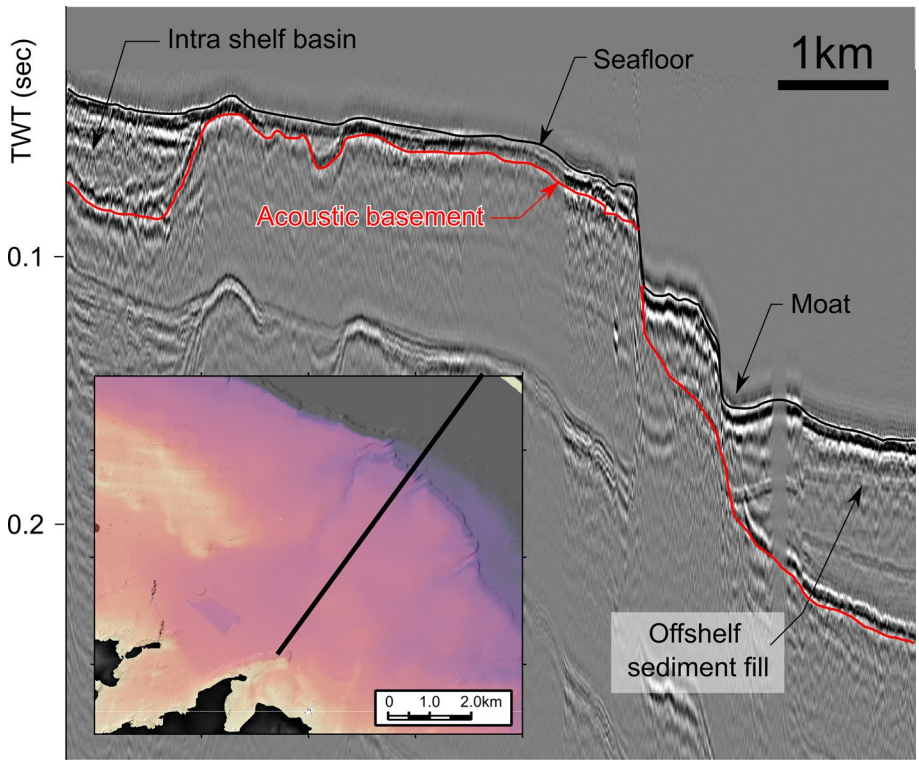


**Fig. 5** Seismic profile across the Maltese shelf (see inset and Fig. 2A, map is north oriented). Seafloor and acoustic basement are delineated. Sediment accumulation across most of the shelf is very thin, thickening in the SE intra-shelf sand basin and off shelf to the NE

## Water column structure

Based on the data from nearby Sicily, the local wave regime displays its mean wave impact depth very close to the surface (Fig. 3). Some 90% of the mean period waves have a wavelength between 30 and 40 m, limiting their wave base depth to ~ 15—20 mbsl (Allen 1985). The peak period does extend to nearly 200 m and would thus place the maximum depth of wave base during extreme events at ~ 110 mbsl. However, most peak period events have a wavelength of no more than 100 m, suggesting that wave activity below 50 mbsl is extremely rare.

Based on CTD data the upper 200 m of the water column in the study area can be divided into three main intervals (Fig. 2, Supplement 2): 1. a surface mixed layer between 0 and 25 mbsl marked by high temperatures (> 26 °C) during the summer; 2. a pycnocline layer, located between ~ 25 and ~ 60 mbsl, that has a variable salinity that overlaps with the thermocline and 3. a sub-pycnocline water mass located below ~ 60 mbsl, marked by increasing density and salinity paired with decreasing temperatures. The maximum Brunt–Väisälä frequencies, ranging between 0.03 and 0.05 Hz, overlap with the pycnocline, whereas below it, the frequencies are between 0.01 and 0.02 Hz.

## Seafloor imagery

Detailed imagery of the seafloor (see Supplement 1 for more information) shows that the main types of seafloor morphology highlighted by low-resolution techniques actually consist of a complex mosaic of multiple sedimentary features. An exception to this pattern seems to be represented by the sand flats area, where AUV photographs (Fig. 6A) show a relatively uniform domain consisting of biogenic sand with sparse fleshy algae and echinoids.

The seafloor in seagrass meadows, where surveyed in detail, was covered by small patches of seagrass (*Posidonia oceanica*) surrounded by biogenic sand (Fig. 6B). This

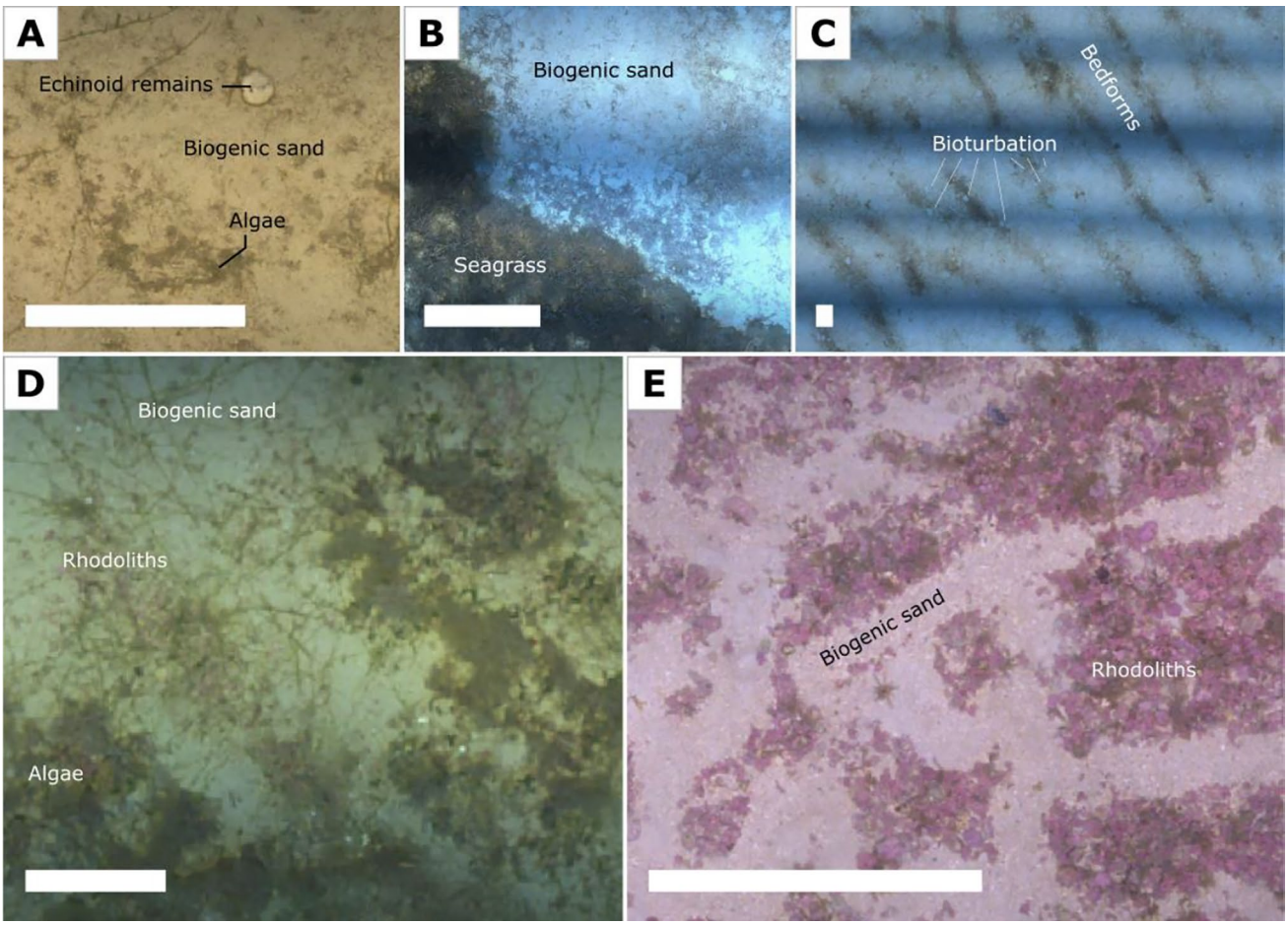


**Fig. 6** Composite mosaics of seafloor imaging of the Maltase shelf (see Fig. 1 for locations) showing different characters of the seafloor (see Supplement 1 for more information). **A** Biogenic sand with echinoid remains (Dive 4); **B** Interface between biogenic sand and seagrass (Dive 2); **C** Sandy bedforms (Dive 2); **D** Clumps of fleshy algae with rhodoliths and calcareous sand (Dive 1); **E** Rhodolith accumulations (Dive 3). All seafloor mosaics are north-oriented

biogenic sand forms bedforms of various sizes, generally oriented with a NW–SE strike (Fig. 6C). In some locations the bedforms are punctuated by resurfacing, that is to say the sediment surface has been reworked and any seaweed has been removed. Bioturbation features are generally common but current-related features are rare (Fig. 6C, Supplement 1).

In areas of rhodolith and maerl beds, more variety was observed. In shallow water, coralline algae are locally interspersed with patches of non-calcareous algae (Fig. 6D). In deep water there are fewer non-calcareous algae and a higher density of coralline algae, with the latter displaying a stronger colour (Fig. 6E). The rhodoliths are usually aligned, developing NW–SE striking bedforms.

## Sediment constituents

All samples collected and analyzed within this study were poor in silt (0% to 5.5%) with most grains being in the sand (higher than 90% in 22 out of 33 samples) or gravel fractions. The mean grain size ranges between 0.2 and 21.6 mm (mean = 2.8 ± 5.6 mm, n = 33), with a standard deviation ranging between 0.1 and 11 mm (mean = 2.1 ± 3.3 mm, n = 33), and skewness ranging between 0.3 and 14.6 (mean = 3.9 ± 2.7, n = 33). With the exception of two samples (samples 29 and 30), all samples exhibit a positive skewness. Mean grain size, standard deviation, %sand, and %gravel do not exhibit any correlation to water depth or distance from shore. The silt percentage is generally higher in shallower water and closer to the shore, whereas the gravel percentage is higher in most distal sites (Fig. 7a). Skewness exhibits a weak non-linear correlation with both water depth ($r = -0.43$, $p = 0.01$) and distance from shore ($r = -0.45$, $p < 0.01$), whereas log skewness increases inversely in both.

When applying the updated Dunham classification of sedimentary texture (Embry and Klovan 1971; Lokier and Al Junaibi 2016), shelf samples are classified as grainstones

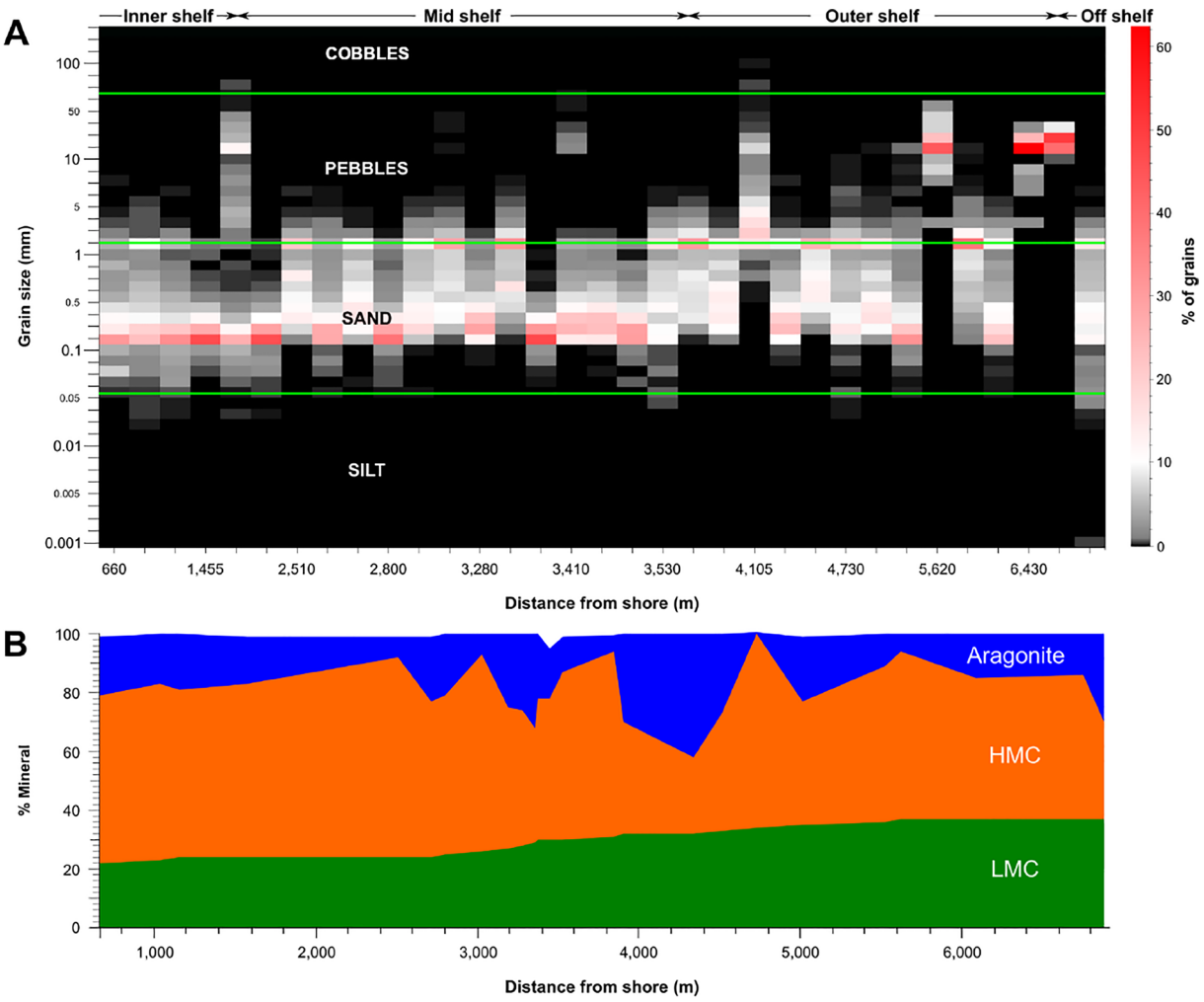


**Fig. 7** Distribution of sediment parameters across the shelf. **A** Grain-size distribution along a gradient away from shore. **B** Carbonate mineral ratios across the shelf from the shore

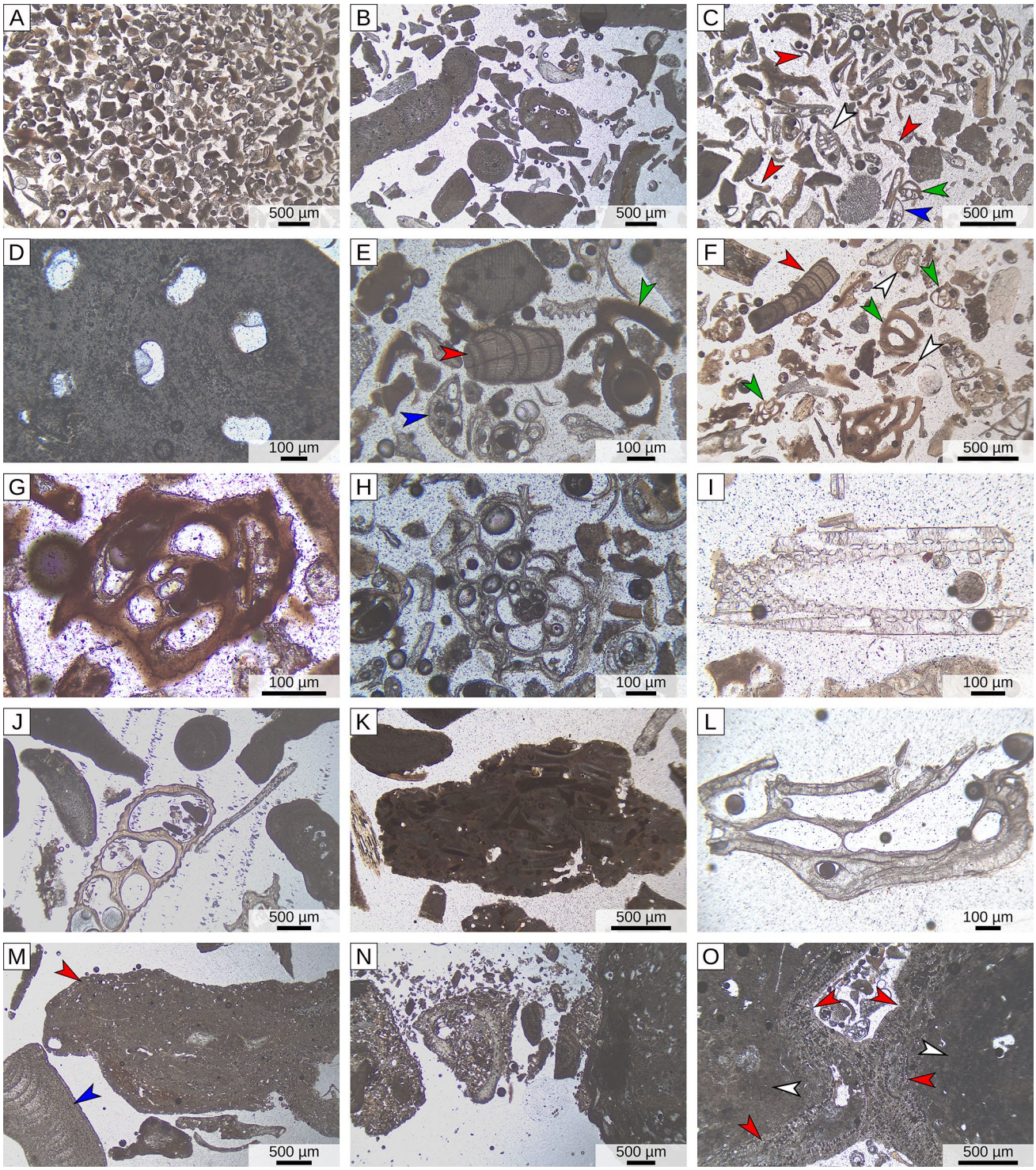


(12 samples), packstones (10 samples, of which sample 31, off the shelf, was the only one that was not poorly washed), floatstones with a grainstone matrix (4 samples), rudstones (6 samples) and bafflestone (1 sample). Under preliminary visual inspection, the most common components in all of these classes of sediment texture are unidentified bioclasts (either pale or dark brown in colour) and coralline algae (which are commonly the dominant type of bioclast). Coralline algae occur as branches (common in samples 11, 12, 19 and 26) and nodules (common in sample 8, but also prevalent in samples 19–21, 24–30 and 30), including rhodoliths (dominant in sample 30) of various sizes (commonly > 1 cm). Less abundant components are represented by foraminifera (notably common in nearshore samples 2,

◂**Fig. 8** **A** Sample 4, dominated by finely comminuted and well-sorted unidentifiable bioclastic fragments. **B** Sample 23, dominated by coralline algae. **C** Sample 18, dominated by finely comminuted and well-sorted bioclastic fragments, several of these fragments are fragments of miliolids (red arrowheads); white arrowhead = *Elphidium*; green arrowhead = small miliolid; blue arrowhead = *Cibicides*. **D** Sample 24, *Phymatolithon calcareum* a coralline alga belonging to the Hapalidiales order. **E** Sample 18, a fragment of an articulated coralline alga (red arrowhead); blue arrowhead = small rotaliid, possibly *Asterigerinata*; green arrowhead = small miliolid. **F** Sample 2 displaying common small miliolids (green arrowhead) and small miliolid fragments (white arrowheads); red arrowhead = articulate coralline alga. **G** Sample 15, *Triloculina*. **H** Sample 13, *Planorbulina*. **I** Sample 22, irregular echinoid spine. **J** Sample 12, rich in pristine coralline algae and molluscs. **K** Sample 7, *Halimeda*. **L** Sample 21, bryozoans. **M** Sample 19 characterized by common reworked grains including coralline algal fragments displaying extensive microborings (red arrowhead); blue arrowhead = pristine coralline alga. **N** Sample 28, dominated by reworked grains of poorly lithified floatstone. **O** Sample 26, a coralline algal nodule consisting of a thin outer layer of recent coralline algae (red arrowheads) growing over a nucleus consisting of micritized coralline algae (white arrowheads)

3 and 4 as well as in sample 31), bryozoans (common in sample 29), and echinoids. Bivalves, gastropods (common in sample 20), pteropods (absent off shelf but present in samples 4, 8, 14, 13, 17, 18 27 and 35) and serpulids (samples 5, 6, 10, 11, 18 and 31); fragments of *Halimeda* (usually poorly preserved) occur in certain samples. *Cladocora* is generally rare except in sample 9, located at the boundary between the *Posidonia* meadows and the sand flats, where it is dominant. No living samples of *Cladocora* were recovered. The distribution of the grains does not exhibit any clear trend, although foraminifera are somewhat more common in the inner shelf, *Halimeda* in the mid-shelf, and coralline algae in the outer shelf. Non-calcareous algae and seagrass fragments were found in 13 samples in water depths between 28 and 69 mbsl. Seagrass debris was primarily found in poorly-washed grainstones to floatstones, whereas algal remains were found within all sedimentary types (Supplement 3).

Based on XRD analyses, the sediments consist, in order of abundance, of HMC, aragonite and low Mg calcite (LMC). No significant amount of clay or quartz was detected in the samples. HMC ranges between 43 and 93% (mean = 63 ± 11%, n = 26), aragonite between 1 and 42% (mean = 19 ± 10%, n = 26) and LMC between 7 and 25% (mean = 18 ± 4, n = 26). LMC increases with the distance from the shore (Fig. 7B) and occurs in all samples, including those comprised purely of coralline algae. Aragonite is more abundant in the mid-shelf rather than the inner or outer shelf.

Point counting analysis of the thin sections confirms the results of preliminary visual analysis with unidentifiable bioclastic fragments (0% to 67.3%, mean = 29.4 ± 18.5%, n = 26) and coralline algae (0.3% to 95%, mean = 41.6 ± 30.7%, n = 26) being the most common components (Figs. 8A and B). By comparing the results of the preliminary visual analysis with those of the point counting of thin sections it becomes clear that at least a part of the unidentifiable bioclastic fragments observed under the stereomicroscope (especially in samples collected close to the shore) are actually finely comminuted remnants of benthic foraminifera (mainly miliolids) (Fig. 8C). Coralline algae are mainly represented by encrusting Corallinales and Hapalidiales (including *Phymatolithon calcareum*) (Fig. 8D), whereas Sporolithales are extremely rare. In samples close to the coast articulated coralline algae are also present (Fig. 8E and F). Benthic foraminifera are abundant (0% to 37%, mean = 13 ± 11%, n = 26), especially close to the coast. They are mainly represented by small miliolids (*Triloculina*, *Quinqueloculina*, *Spiroloculina*) (Fig. 8F and G), encrusting miliolids (nubeculariids), and small rotaliids (*Ammonia*, *Elphidium*, *Asterigerinata*, *Cibicides*) (Fig. 8C and E). Large rotaliids are less common and mainly represented by specimens of *Planorbulina, Planorbulina* also occurs (Fig. 7H). Echinoderms are mainly represented by elements of irregular echinoids close to the coast (Fig. 7I) and by regular echinoids more offshore. Molluscs (mainly gastropods and bivalves) commonly occur in most samples and they can be locally significant (Fig. 8J). The contribution from *Halimeda*, bryozoans, serpulids and ostracods is usually minor (Fig. 8K and L). *Cladocora* is only present in sample 9.

## Statistical analysis of sedimentary composition

By analyzing these data, it is apparent that the abundance of several constituents exhibits a near linear decline with distance from shore (and similarly to water depth). These notably include unidentifiable bioclastic fragments ($r = -0.47$, $p = 0.02$), echinoids ($r = -0.47$, $p = 0.02$), rotaliids ($r = -0.58$, $p < 0.01$) and miliolids ($r = -0.62$, $p < 0.01$). The abundance of *Halimeda* negatively correlates with water depth ($r = -0.55$, $p < 0.01$) but not with the distance from shore ($r = -0.31$, $p > 0.05$). Coralline algae exhibit an opposite trend and increase with depth ($r = 0.60$, $p < 0.01$) and distance from shore ($r = 0.66$, $p < 0.01$). The abundance of molluscs, bryozoans, serpulids, ostracods and textulariids does not exhibit any correlation to water depth or distance from shore. However, mollusc abundance is higher in the mid shelf. No parameter appears to correlate with the intensity of the seafloor backscatter (the amount of energy / strength a of the signal coming back from a part of the seafloor, reflecting the surface characteristics in a statistically significant fashion). Several components exhibit strong correlations to each other, e.g. the abundance of echinoids correlates with both the abundance of miliolids ($r = 0.71$, $p < 0.01$), rotaliids ($r = 0.88$, $p < 0.01$) and of unidentifiable bioclastic fragments ($r = 0.72$, $p < 0.01$).

To further elucidate these relations, multi-variant analysis was carried out using detrended correspondence analysis (DCA) and non-metric multi-dimensional scaling

(nMDS) using Bray–Curtis indices on the results of thin-section analysis. Axis 1 and 2 of the analysis account for eigenvalues of 0.41 and 0.06, respectively. The principle loading on axis 1 of the DCA (Fig. 9A) is represented by the ratio between red calcareous algae (RCA) and all other components. Axis 2 represents miliolids, rotaliids, serpulids, and sponge spicules vs. all other components other than RCA. RCA have a minimal loading on axis 2. The result of the MDS analysis (Fig. 9B) has a stress of 0.02. The loading on axis 1 is positive for coralline algae, molluscs, bryozoans and textulariids, negative for anything else. Axis 2 has instead a positive loading from echinoids, unidentified bioclasts, molluscs and textulariids, and negative for anything else.

Thin-section analyses also indicate that, alongside recent grains, reworked grains represent a sizable proportion of the investigated sediments (Fig. 8M–O). They consist of either bioclasts displaying extensive borings and micritization (Fig. 8M) or of lumps of poorly lithified material (packstone to floatstone textures) (Fig. 8N). Wherever bioerosion and micritization do not obliterate original structures entirely, reworked assemblages seem to have a composition similar to that of modern assemblages. The overall abundance of reworked grains increases with increasing distance from the shoreline, with most coralline-algal-rich samples dominated by reworked material. This can be clearly noticed in the rhodolith-dominated sample 26, where thin crusts of relatively fresh coralline algae grew over cores consisting of micritized coralline algae whose structures are almost completely obliterated (Fig. 8O).

## Discussion

### Sedimentary facies of the Maltese shelf

The Holocene sedimentary cover atop the Maltese shelf is, for the most part, a thin veneer upon the glacial truncation surface (Fig. 5). This resulted in many terrestrial features, such as palaeochannels and local basins (Fig. 4B), punctuating the shelf (Micallef et al. 2013). Prior acoustic mapping of the seafloor (Micallef et al. 2012, 2013) identified that these relict features host relict facies whose recent counterparts currently occur elsewhere on the shelf, organized in distinct facies belts. Our analysis of seafloor imaging highlights the presence of three of these facies in the study area (Fig. 10): an inner-shelf seagrass facies related to meadows (Fig. 6B) and characterised by a packstone to grainstone texture; a middle-shelf sand-flat facies (mostly occurring in relict troughs) characterised by a grainstone to floatstone texture (Fig. 5A); an outer-shelf rhodolith and maerl bed facies (Fig. 6E) characterised by a grainstone to rudstone texture. Farther offshore, outside of the bathymetric range considered for the current paper and outside of the study area, lies an off-shelf domain that hosts additional facies in the form of coralligenous (commonly calcareous red algae) buildups (mainly occurring southeast of the Island) and off-shelf sediments characterised by a packstone texture (Bialik et al. 2022).

This high-order facies classification does not translate directly to sediment compositions. The sediment composition across the inner and mid shelf, corresponding to the

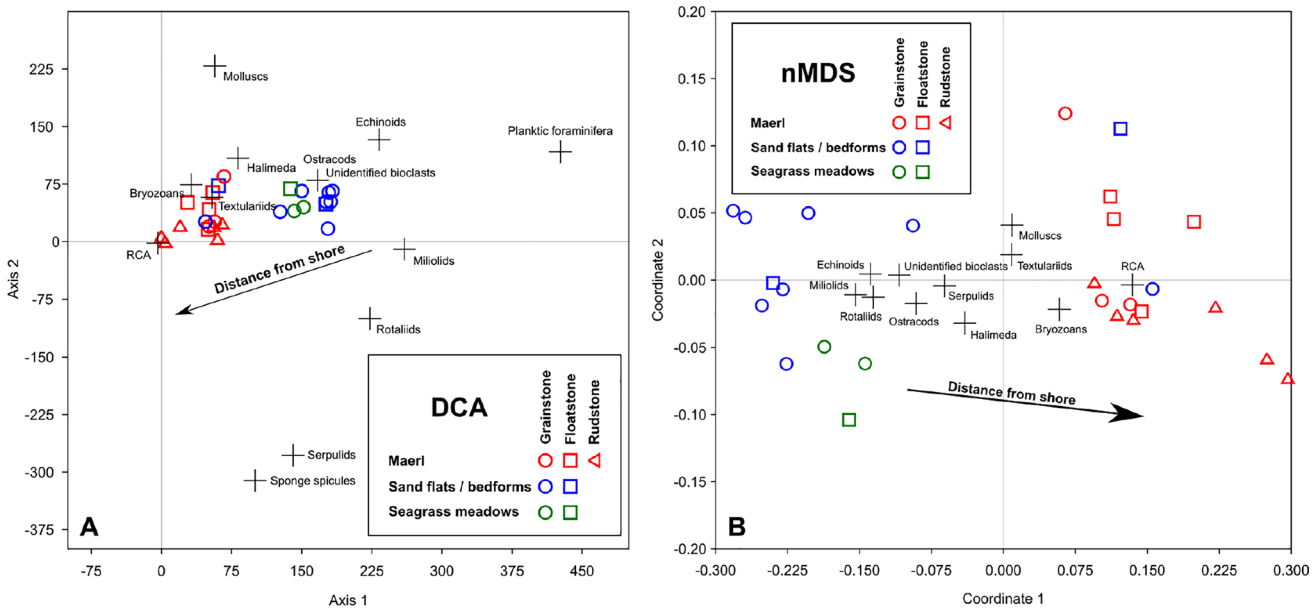


**Fig. 9** **A** DCA and **B** nMDS ordination analysis of point counts in thin sections. Both analyses indicate a gradient away from shore

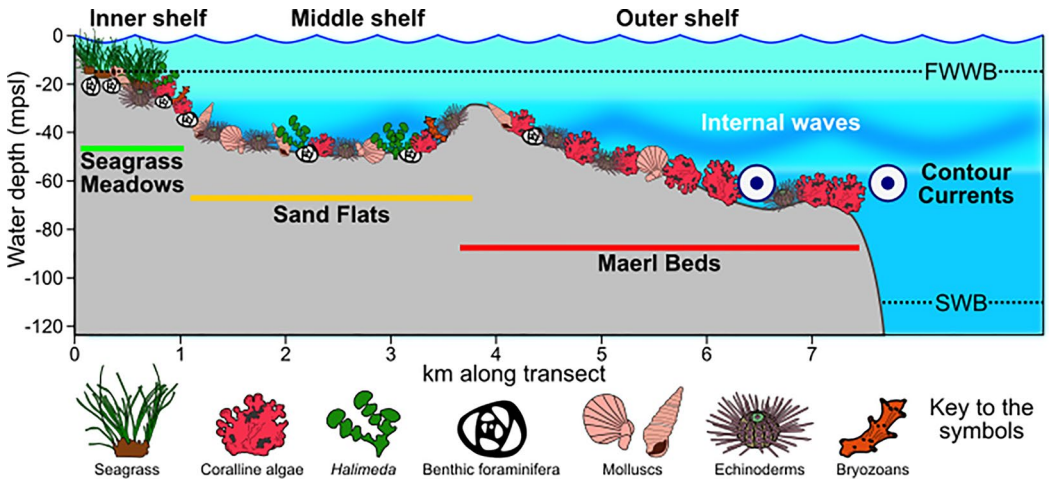


**Fig. 10** Schematic model of the facies present across the Maltese shelf and the main governing parameters on sediment distribution

seagrass meadow and the sand flat facies, exhibits the same grain assemblage (benthic foraminifera, molluscs, echinoids, *Halimeda*, bryozoans, coralline algae and a large amount of unidentifiable bioclasts). The abundance of most of these grains diminishes with distance from shore, irrespective of the acoustic facies, with some components (e.g., *Halimeda*) being dependent only on water depth. In the DCA analysis, the samples from the seagrass meadows cannot be clearly differentiated from those of the sand flats, (Fig. 9A). Some separation can be observed in the nMDS (Fig. 9B). Based on grain size and mineralogical composition (Fig. 7) some differentiation between seagrass meadow and sand flat samples is clear. The samples from the seagrass meadow host a silt-sized fraction that is almost entirely absent in sand-flat samples. Seagrass meadow samples are also characterized by a higher abundance of HMC compared to sand-flat samples. The latter are also richer in aragonite compared with samples from the other two facies. Seafloor vegetation plays an important role in the retention of fine-grained material on Mediterranean shelves (De Falco et al. 2003; Hendriks et al. 2010). Through physical baffling and reduction of current velocities (Fonseca and Koehl 2006; Mateu-Vicens et al. 2012), seafloor vegetation allows a wide range of grain sizes to be retained in the proximal region of the shelf (Fonseca and Koehl 2006; Mateu-Vicens et al. 2012). The prevalence of fleshy algae and seagrass close to shore (Figs. 4B, 6B and D) is the likely reason why any silt-sized grains could be retained in the region of the shelf mostly affected by wave activity. At present, the distribution of seagrass is highly affected by anthropogenic activities such as coastal development, pollution, trawling, fish farming, moorings, dredging and dumping (Boudouresque et al. 2009; Telesca et al. 2015; Beca-Carretero et al. 2020). Excluding these impacts and assuming that salinity and nutrient state on a small region such as the Maltese shelf are relatively uniform, the distribution of seagrasses should be primarily light-dependent (Vizzini 2009; Bernardeau-Esteller et al. 2015). This would limit the distribution of the seagrass meadow facies only to shallow water as observed here and elsewhere in the Mediterranean (De Falco et al. 2011; Vacchi et al. 2017).

While the baffling effect of meadows can explain the retention of fine grains in shallow waters, it does not explain the absence of fine grains in deeper water. Wavelength estimation from wave periods (Clifton and Dingler 1984) of the Italian RON (Bencivenga et al. 2012) buoy of Mazara del Vallo (offshore southern Sicily) indicates that maximum wave impact depth on the shelf (which roughly corresponds to half wavelength, Allen 1985) should occur at about 110 mbsl. This will be considered here as our storm wave base (SWB), although it must be stressed that most of storm waves have a shorter wavelength, suggesting that wave activity below 50 mbsl is limited. Based on the 80% to 90% cumulative frequency cut-off of the mean period we estimate the FWWB to be at around 15–20 mbsl (Fig. 3A). Therefore, since most of wave energy is dissipated in the shallow-water of the inner shelf (Fig. 3) and there are only about 30 days of storms a year in Malta (Grabowska 2010), fine grains in middle and outer shelf areas are probably winnowed by two main process other than waves: internal waves and bottom currents. Given that the maximum Brunt–Väisälä frequencies (indicating the potential capacity to propagate internal waves) are between ~ 25 and ~ 60 mbsl (Fig. 2) it is unlikely that the winnowing in the outer shelf is dominantly caused by internal waves as the impact of the latter will be focused at the maximum buoyancy boundary defined by the high Brunt–Väisälä frequencies (i.e. around 30 to 60 mbsl, overlying the pycnocline). That said, pycnocline depth does overlap with the larger sandy bedforms in the mid-shelf (Fig. 4B), which is presently below the fair-weather wave base, and, therefore, is likely a mechanism in shaping

these bedforms. Since the CTD data were collected in the late summer, when the thermocline is at its deepest before breaking due to winter mixing, there is a low probability of this interface occurring at a greater depth in other seasons.

Although internal waves may explain part of the winnowing at around 30 to 60 mbsl, just below FWWB, another cause for the winnowing observed in deeper water is required. The linear arrangements of the rhodolith accumulations would suggest transport along the strike of the shelf, such as the one that would be generated by a contour current. The moat at the base of the escarpment (Fig. 5) would also support the existence of a shelf-parallel bottom current. In the low likelihood of internal waves and storm waves at this depth (see above), contour currents are a more likely mechanism for the winnowing. Such currents would be in line with the regional flow regime, notably during summer (Reyes Suarez et al. 2019).

Coralline nodule-rich facies (rhodolith and maerl beds) are abundant in mesophotic depths in the central Mediterranean, but both the characteristics of the facies and of the nodules are highly variable (De Falco et al. 2011; Bracchi and Basso 2012; Savini et al. 2012; Sañé et al. 2021). Across the Maltese shelf coralline algal nodules exhibit a wide range of sizes and morphologies as well as a variable amount of living calcareous algal fraction (Sciberras et al. 2009). The specific controls on the morphology of the nodules are not perfectly clear. However, the intermittent growth observed in the investigated nodules, with termination, stasis and later reestablishment (Fig. 8O), may be the result of strong storm events (Dulin et al. 2020). These storms may also impact the transport of the coralline nodules into deeper water. Coralline algae prefer low levels of fines and low light conditions (Leukart and Lüning 1994; Villas-Bôas et al. 2014; Coletti et al. 2018). Indeed Mediterranean rhodolith and maerl beds mainly occur around islands, capes, on the top of submarine plateaus, and in areas influenced by strong tidal currents (Basso et al. 2017). All these environments, either due to the lack of clastic input or due to currents clearing the sediment, are characterized by a low sedimentation rate. In the case of the Maltese shelf, both the reduced input of sediment from the coast, caused by the arid climate, and the presence of currents on the outer shelf might favour the development of this facies. The dominance of coralline algae in the outer shelf is, in turn, also one of the reasons for the increase in the gravel percentage moving away from the coast (Fig. 6a). While the seagrass-related factory that dominates close to the coast mainly produces sand-sized material (Frezza et al. 2011), coralline-algal factories mostly produce coarse-grained bioclasts (Pomar 2001). Furthermore, the higher hydrodynamic energy of the coastal sector would promote the fragmentation of bioclasts, resulting in abundant fine-sand-sized material close to the coast. On the other hand, in the outer shelf characterized by the rhodolith and maerl bed facies (maerl beds sensu Micallef et al. 2012), the reduced effect of waves would hinder wave-related fragmentation and thus the production of sand and mud-sized bioclasts.

Grains derived from *Halimeda* were found in the sediment. However, despite it being reported as a very common alga in the Maltese shelf in the mid-twentieth century (Larkum et al. 1967), no living *Halimeda* were observed in the AUV, vCTD or grab samples. Interviews carried out with the local diving communities confirm some presence of *Halimeda* on the shelf, but occurrences are rare and in small amounts. It is possible that this major contributor has been suppressed in recent years as part of the ongoing species collapse observed in the Mediterranean (Rilov 2016; Albano et al. 2021). The disparity between the abundance of *Halimeda* grains and of living *Halimeda* suggests long retention time of grains in the sedimentary system. This is similarly confirmed by the reworking of coralline nodules and the significant abundance of reworked bioclastic grains across the Maltese shelf. This long retention time may allow for recrystallization, which would account for the high fraction of LMC in the sediment, notably in the outer shelf (Fig. 7B).

## Controls on sediment and facies distribution on the I/C-type carbonate platform

Energy availability, either from the sun or the breakdown of the organic matter from ingested food is the main parameter governing and limiting the distribution of grains on the global scale (Bialik et al. 2023). The availability of these two main types of energy, in turn, is related to abiotic parameters such as light availability, water clarity, nutrient abundance, temperature and currents (Halfar et al. 2004; Michel et al. 2019; Laugié et al. 2019; Reijmer 2021). These parameters also play an important role on the smaller scale, together with marine connectivity and local control over sediment transport (Gischler 2006, 2010, 2020; Jarochowska 2012; Schmitt and Gischler 2017). In this regard, the Maltese shelf displays similarities with other Mediterranean carbonate systems that are characterized by warm-temperate oligotrophic water (Pérès and Picard 1964; Carannante et al. 1988). Both on the Tyrrhenian (Basso 1998; Brandano and Civitelli 2007; Frezza et al. 2011; De Falco et al. 2011; Bracchi and Basso 2012) and Balearic shelves (Fornós and Ahr 2006), shallow settings are dominated by carbonate factories related to seagrasses and algal meadows and characterized by abundant epiphytic production. Deeper settings are instead usually dominated by coralline-algal factories. Farther offshore, the contribution of pelagic fallout becomes increasingly relevant.

The Maltese shelf differs from the Balearic and Tyrrhenian examples as meadows extend to at least 45 mbpsl (Supplements 1, 3) and meadow-related sediments extend farther offshore and into deeper water (Mateu-Vicens et al.

2012; Benedetti and Frezza 2016). The larger extensions of meadow-related deposits compared to Balearic and Tyrrhenian locations could be caused by the limited siliciclastic supply occurring on the Maltese shelf. As the island is small, mainly consisting of limestone, and characterized by an arid climate, the terrigenous supply to the shelf is limited. Limited terrigenous input is also indicated by the LMC fraction in the sediments. The erosion of Malta's limestone should mainly supply LMC. This is suggested by the composition of sediments from embayed beaches, which mostly derive from the erosion of the coastal limestone and mainly consist of LMC (Gatt 2021). Therefore, a significant terrigenous influx from the land should be matched by a peak of LMC close to the coast. This peak is not observed (Fig. 7B).

Previous authors, based on the overall percentage of carbonate, suggested that most of the carbonate production along the Tyrrhenian and Balearic shelves occur in coralline-algal-dominated, facies (Brandano and Civitelli 2007; Bracchi and Basso 2012). However, as noted by Fornos and Ahr (2006), there is a significant difference between production rates and accumulation rates. Relying only on the latter could be misleading. Furthermore, the percentage of carbonate is the result of both the bioclastic and siliciclastic accumulation rates. Low accumulation rates of siliciclastic detrital material might result in almost pure carbonates even with a limited rate of bioclastic production. Across the Maltese shelf the abundance of old and reworked material in coralline-algal dominated sediments indicate long exposure of the bioclasts on the seafloor and an overall low accumulation rate. This stresses the need for further studies aimed at assessing accurate accumulation and production rates of both coralline-algal and epiphytic carbonate factories in the Mediterranean and elsewhere. The relevance of the epiphytic carbonate factory seems to be also one of the main differences that separate the Maltese shelf from other systems dominated by C-type factories, like those offshore Brazil.

Similarly to Mediterranean systems, the outer shelf of many south Atlantic systems is dominated by coralline algae (Carannante et al. 1988; Testa and Bosence 1999; Vale et al. 2018). On the other hand, nearshore, these systems are usually characterized by a siliciclastic-dominated zone (Testa and Bosence 1999). Still in shallow water but away from the main sources of siliciclastic sediment, carbonate production is dominated by *Halimeda*, coralline algae and, locally, by hermatypic corals (Testa and Bosence 1999). While seagrass and seaweed meadows are reported along the Brazilian coast (Testa and Bosence 1999; Gomes et al. 2015), their prevalence seems to be lower in comparison to the central Mediterranean. Since porcelaneous foraminifera seem to represent a significant output of these vegetated factories, they could be critical in differentiating, within geological deposits, between the different modes of C-type factories (i.e., Atlantic-like or Mediterranean-like). Unfortunately, their thin HMC test can be easily dissolved during diagenesis, limiting the possibility of actually recognizing seagrass or seaweed-related facies in the fossil record unless other indicators (e.g., large encrusting rotaliids) are also preserved (Reich et al. 2015; Mariani et al. 2022).

## Conclusions

The Maltese shelf is primarily an l/C-type carbonate platform. Based on visual inspection, three main facies can be discerned across the investigated portion of the Maltese shelf (Fig. 10): seagrass meadows, sand flats and rhodolith and maerl beds. However, these facies are not clearly separated in terms of sedimentary composition. The sediment along the shelf is dominated by reworked unidentifiable bioclasts associated with coralline algae, benthic foraminifera (notably small miliolids) and echinoderms. The distribution of these components along the shelf varies but as a gradient rather than as clearly marked changes. This gradient is characterised by increasing grain size and LMC with increasing depth and a transition from green to red calcareous algae. Light and hydrodynamic energy (whose effects are in turn controlled by seafloor morphology) are the main elements governing this facies distribution. Waves and seagrass baffling are mainly effective in the inner shelf; internal waves are relevant on the middle shelf, and contour currents on the outer shelf. A low rate of terrigenous sedimentation also contributes to the system, favouring the development of extensive seagrass meadows close to the coast and rhodolith and maerl beds more off-shore. These extensive seagrass meadows are notably different from the Brazilian depositional systems which are also characterised by C-type factories, but display limited sediment contribution from epiphytic production. While l/C-type carbonate factories, similar to modern Mediterranean ones, are not prevalent now, they were highly abundant around the Tethys through most of the Cenozoic and these findings should be taken into account when interpreting these environments in the future.

**Supplementary Information** The online version contains supplementary material available at https://doi.org/10.1007/s10347-024-00690-1.

**Acknowledgements** The first author is currently supported by Marie Skłodowska Curie fellowship (101003394—RhodoMalta). Ship time was funded by Helmholtz European Partnering project SMART. CB, MS and AM took part in Sonne expedition SO277, collecting primary data used in this cruise. The surveys were possible following permits issued by the Continental Shelf Department, the Environment and Resources Authority, the Superintendence of Cultural Heritage, and the Ports and Yachting Directorate. The authors would like to thank editor Maurice Tucker for his patience and help with this manuscript as well as to two anonymous reviewers for their input.

**Funding** Open access funding provided by Università degli Studi di Milano - Bicocca within the CRUI-CARE Agreement.

**Data availability** Information and links to external repository with the data is already in the text.

## Declarations

**Conflict of interest** The authors declare no conflict of interests.

**Open Access** This article is licensed under a Creative Commons Attribution 4.0 International License, which permits use, sharing, adaptation, distribution and reproduction in any medium or format, as long as you give appropriate credit to the original author(s) and the source, provide a link to the Creative Commons licence, and indicate if changes were made. The images or other third party material in this article are included in the article's Creative Commons licence, unless indicated otherwise in a credit line to the material. If material is not included in the article's Creative Commons licence and your intended use is not permitted by statutory regulation or exceeds the permitted use, you will need to obtain permission directly from the copyright holder. To view a copy of this licence, visit http://creativecommons.org/licenses/by/4.0/.

## References

Adam J, Reuther C-D, Grasso M, Torelli L (2000) Active fault kinematics and crustal stresses along the Ionian margin of southeastern Sicily. Tectonophysics 326:217–239. https://doi.org/10.1016/S0040-1951(00)00141-4

Albano PG, Steger J, Bošnjak M et al (2021) Native biodiversity collapse in the eastern Mediterranean. Proc R Soc B Biol Sci 288:20202469. https://doi.org/10.1098/rspb.2020.2469

Allen JRL (1985) Principles of physical sedimentology. Chapman and Hall, London

Alongi DM (1989) Benthic processes across mixed terrigenous-carbonate sedimentary facies on the central Great Barrier Reef continental shelf. Cont Shelf Res 9:629–663. https://doi.org/10.1016/0278-4343(89)90034-4

Bassi D, Nebelsick JH (2010) Components, facies and ramps: Redefining Upper Oligocene shallow water carbonates using coralline red algae and larger foraminifera (Venetian area, northeast Italy). Palaeogeogr Palaeoclimatol Palaeoecol 295:258–280. https://doi.org/10.1016/j.palaeo.2010.06.003

Basso D (1998) Deep rhodolith distribution in the Pontian Islands, Italy: a model for the paleoecology of a temperate sea. Palaeogeogr Palaeoclimatol Palaeoecol 137:173–187. https://doi.org/10.1016/S0031-0182(97)00099-0

Basso D, Babbini L, Ramos-Esplá AA, Salomidi M (2017) Mediterranean rhodolith beds. In: Riosmena-Rodríguez R, Nelson W, Aguirre J (eds) Rhodo- lith/Maërl Beds: a global perspective. Springer, Cham, pp 281–299

Beca-Carretero P, Teichberg M, Winters G et al (2020) Projected rapid habitat expansion of tropical seagrass species in the mediterranean sea as climate change progresses. Front Plant Sci. https://doi.org/10.3389/fpls.2020.555376

Ben Ismail S, Sammari C, Pietro GG et al (2012) Water masses exchanged through the Channel of Sicily: evidence for the presence of new water masses on the Tunisian side of the channel. Deep Sea Res Part I Oceanogr Res Pap 63:65–81. https://doi.org/10.1016/j.dsr.2011.12.009

Bencivenga M, Nardone G, Ruggiero F, Calore D (2012) The Italian data buoy network (RON). In: Rahman M, Brebbia CA (eds) Advances in Fluid Mechanics IX. p 305

Benedetti A, Frezza V (2016) Benthic foraminiferal assemblages from shallow-water environments of northeastern Sardinia (Italy, Mediterranean Sea). Facies 62:1–17. https://doi.org/10.1007/s10347-016-0465-9

Bergman KL, Westphal H, Janson X et al (2010) Controlling parameters on facies geometries of the bahamas, an isolated carbonate platform environment. In: Westphal H, Riegl B, Eberli GP (eds) Carbonate depositional systems: assessing dimensions and controlling parameters. Springer, Netherlands, Dordrecht, pp 5–80

Bernardeau-Esteller J, Ruiz JM, Tomas F et al (2015) Photoacclimation of *Caulerpa cylindracea*: Light as a limiting factor in the invasion of native Mediterranean seagrass meadows. J Exp Mar Bio Ecol 465:130–141. https://doi.org/10.1016/j.jembe.2014.11.012

Berndt C, Urlaub M, Jegen M, et al (2021) RV SONNE Fahrtbericht / Cruise Report SO277 OMAX: Offshore Malta Aquifer Exploration. Keil

Betzler C, Lindhorst S, Lüdmann T et al (2015) The leaking bucket of a Maldives atoll: Implications for the understanding of carbonate platform drowning. Mar Geol 366:16–33. https://doi.org/10.1016/j.margeo.2015.04.009

Bialik OM, Jarochowska E, Grossowicz M (2021) Ordination analysis in sedimentology, geochemistry and palaeoenvironment—Background, current trends and recommendations. Depos Rec 7:541–563. https://doi.org/10.1002/dep2.161

Bialik OM, Varzi AG, Durán R et al (2022) Mesophotic depth biogenic accumulations "Biogenic Mounds" Offshore the Maltese Islands, Central Mediterranean Sea. Front Mar Sci. https://doi.org/10.3389/fmars.2022.803687

Bialik OM, Coletti G, Mariani L et al (2023) Availability and type of energy regulate the global distribution of neritic carbonates. Sci Rep 13:19687. https://doi.org/10.1038/s41598-023-47029-4

Biolchi S, Furlani S, Antonioli F et al (2016) Boulder accumulations related to extreme wave events on the eastern coast of Malta. Nat Hazards Earth Syst Sci 16:737–756. https://doi.org/10.5194/nhess-16-737-2016

Bishop WF (1988) Petroleum geology of East-Central Tunisia. Am Assoc Pet Geol Bull 9:1033–1058

Bosellini FR, Perrin C (2008) Estimating Mediterranean Oligocene-Miocene sea-surface temperatures: an approach based on coral taxonomic richness. Palaeogeogr Palaeoclimatol Palaeoecol 258:71–88. https://doi.org/10.1016/j.palaeo.2007.10.028

Bosence DWJ, Pedley MH (1982) Sedimentology and palaeoecology of a Miocene coralline algal biostrome from the Maltese Islands. Palaeogeogr Palaeoclimatol Palaeoecol 38:9–43. https://doi.org/10.1016/0031-0182(82)90062-1

Boudouresque CF, Bernard G, Pergent G et al (2009) Regression of Mediterranean seagrasses caused by natural processes and anthropogenic disturbances and stress: a critical review. botm 52:395–418. https://doi.org/10.1515/BOT.2009.057

Bracchi VA, Basso D (2012) The contribution of calcareous algae to the biogenic carbonates of the continental shelf: Pontian Islands, Tyrrhenian Sea, Italy. Geodiversitas 34:61–76. https://doi.org/10.5252/g2012n1a4

Braga JC, Bassi D, Piller WE (2012) Palaeoenvironmental significance of oligocene-miocene coralline red algae - a Review. In: Mutti M, Piller W, Betzler C (eds) Carbonate systems during the oligocene-miocene climatic transition. Wiley-Blackwell, Oxford, UK, pp 165–182

Brandano M, Civitelli G (2007) Non-seagrass meadow sedimentary facies of the Pontinian Islands, Tyrrhenian Sea: a modern example of mixed carbonate-siliciclastic sedimentation. Sediment Geol 201:286–301. https://doi.org/10.1016/j.sedgeo.2007.05.012

Carannante G, Esteban M, Milliman JD, Simone L (1988) Carbonate lithofacies as paleolatitude indicators: problems and limitations. Sediment Geol 60:333–346. https://doi.org/10.1016/0037-0738(88)90128-5

Causon Deguara J, Gauci R (2017) Evidence of extreme wave events from boulder deposits on the south-east coast of Malta (Central Mediterranean). Nat Hazards 86:543–568. https://doi.org/10.1007/s11069-016-2525-4

Clifton HE, Dingler JR (1984) Wave-formed structures and paleoenvironmental reconstruction. Mar Geol 60:165–198. https://doi.org/10.1016/S0070-4571(08)70146-8

Coletti G, Basso D (2020) Coralline algae as depth indicators in the Miocene carbonates of the Eratosthenes Seamount (ODP Leg 160, Hole 966F). Geobios 60:29–46. https://doi.org/10.1016/j.geobios.2020.03.005

Coletti G, Bracchi VA, Marchese F et al (2018) Quaternary build-ups and rhodalgal carbonates along the adriatic and ionian coasts of the Italian peninsula: a review. Riv Ital Di Paleontol e Stratigr 124:387–406

Coletti G, Commissario L, Mariani L et al (2022) Palaeocene to Miocene southern Tethyan carbonate factories: a meta-analysis of the successions of South-western and Western Central Asia. Depos Rec. https://doi.org/10.1002/dep2.204

De MacEdo Dias GT, Villaa RC (2012) Coralline algae depositional environments on the Brazilian central-south-eastern shelf. J Coast Res 28:270–279. https://doi.org/10.2112/11T-00003.1

De Falco G, Molinaroli E, Baroli M, Bellaciccob S (2003) Grain size and compositional trends of sediments from Posidonia oceanica meadows to beach shore, Sardinia, western Mediterranean. Estuar Coast Shelf Sci 58:299–309. https://doi.org/10.1016/S0272-7714(03)00082-9

De Falco G, De Muro S, Batzella T, Cucco A (2011) Carbonate sedimentation and hydrodynamic pattern on a modern temperate shelf: The strait of Bonifacio (western Mediterranean). Estuar Coast Shelf Sci 93:14–26. https://doi.org/10.1016/j.ecss.2011.03.013

Dulin T, Avnaim-Katav S, Sisma-Ventura G et al (2020) Rhodolith beds along the southeastern Mediterranean inner shelf: Implications for past depositional environments. J Mar Syst 201:103241. https://doi.org/10.1016/j.jmarsys.2019.103241

Dunham RJ (1962) Classification of Carbonate Rocks According to Depositional Textures. In: Ham WE (ed) Classification of Carbonate Rocks - A Symposium. AAPG Memoir 1, pp 108–121

Embry AF, Klovan JE (1971) A Late Devonian reef tract on northeastern Banks Island, NWT. Bull Can Pet Geol 19:730–781

Ferraro L, Innangi S, Di Martino G et al (2020) Seafloor features and benthic foraminifera off Linosa Island (Sicily Channel, southern Mediterranean). J Mar Syst 211:103421. https://doi.org/10.1016/j.jmarsys.2020.103421

Fichaut M, Garcia MJ, Giorgetti A et al (2003) MEDAR/MEDATLAS 2002: a mediterranean and black sea database for operational oceanography. In: Dahlin H, Flemming NC, Nittis K, Petersson SE (eds) Building the European capacity in operational oceanography. Elsevier, The Netherlands, pp 645–648

Flügel E (2010) Microfacies of carbonate rocks. Springer, Berlin, Heidelberg

Foglini F, Prampolini M, Micallef A et al (2016) Late quaternary coastal landscape morphology and evolution of the Maltese Islands (Mediterranean Sea) reconstructed from high-resolution seafloor data. Geol Soc Spec Publ 411:77–95. https://doi.org/10.1144/SP411.12

Folk RL (1959) Practical petrographic classification of limestones. Am Assoc Pet Geol Bull 43:1–38

Fonseca MS, Koehl MAR (2006) Flow in seagrass canopies: the influence of patch width. Estuar Coast Shelf Sci 67:1–9. https://doi.org/10.1016/j.ecss.2005.09.018

Fornós JJ, Ahr WM (2006) Present-day temperate carbonate sedimentation on the Balearic Platform, western Mediterranean: Compositional and textural variation along a low-energy isolated ramp. Geol Soc Spec Publ 255:71–84. https://doi.org/10.1144/GSL.SP.2006.255.01.06

Frezza V, Mateu-Vicens G, Gaglianone G et al (2011) Mixed carbonate-siliclastic sediments and benthic foraminiferal assemblages from *Posidonia oceanica* seagrass meadows of the central Tyrrhenian continental shelf (Latium, Italy). Ital J Geosci 130:352–369. https://doi.org/10.3301/IJG.2011.07

Gaglianone G, Brandano M, Mateu-Vicens G (2017) The sedimentary facies of *Posidonia oceanica* seagrass meadows from the central Mediterranean Sea. Facies 63:1–21. https://doi.org/10.1007/s10347-017-0511-2

Galdies C (2011) The climate of Malta: statistics, trends and analysis 1951–2010. National Statistics Office, Malta, Valleta

Garvine RW (2021) The vertical structure and subtidal dynamics. J ofMarine Res 62:337–371

Gatt P (2021) Embayment morphometrics, granulometry and carbonate mineralogy of sandy beaches in the Maltese Islands. Mar Geol 432:106394. https://doi.org/10.1016/j.margeo.2020.106394

Gischler E (2006) Sedimentation on Rasdhoo and Ari Atolls, Maldives, Indian ocean. Facies 52:341–360. https://doi.org/10.1007/s10347-005-0031-3

Gischler E (2010) Sedimentary facies of Bora Bora, Darwin's type barrier reef (Society Islands, South Pacific): the unexpected occurrence of non-skeletal grains. J Sediment Res 81:1–17. https://doi.org/10.2110/jsr.2011.4

Gischler E (2020) Sediments of the almost-atoll Aitutaki, Cook Islands. South Pac Sediment Geol 403:105672. https://doi.org/10.1016/j.sedgeo.2020.105672

Gischler E, Hudson JH, Pisera A (2008) Late Quaternary reef growth and sea level in the Maldives (Indian Ocean). Mar Geol 250:104–113. https://doi.org/10.1016/j.margeo.2008.01.004

Gomes MP, Vital H, Eichler PPB, Gupta BKS (2015) The investigation of a mixed carbonate-siliciclastic shelf, NE Brazil: Side-scan sonar imagery, underwater photography, and surface-sediment data. Ital J Geosci 134:9–22. https://doi.org/10.3301/IJG.2014.08

Grabowska K (2010) Changes in storm frequency in the mediterranean sea region. Misc Geogr 14:71–78. https://doi.org/10.2478/mgrsd-2010-0007

Gutscher M-A, Dominguez S, de Lepinay BM et al (2016) Tectonic expression of an active slab tear from high-resolution seismic and bathymetric data offshore Sicily (Ionian Sea). Tectonics 35:39–54. https://doi.org/10.1002/2015TC003898

Guy-Haim T, Silverman J, Wahl M et al (2020) Epiphytes provide micro-scale refuge from ocean acidification. Mar Environ Res 161:105093. https://doi.org/10.1016/j.marenvres.2020.105093

Halfar J, Mutti M (2005) Global dominance of coralline red-algal facies: a response to Miocene oceanographic events. Geology 33:481–484. https://doi.org/10.1130/G21462.1

Halfar J, Godinez-Orta L, Mutti M et al (2004) Nutrient and temperature controls on modern carbonate production: an example from the Gulf of California. Mexico Geology 32:213. https://doi.org/10.1130/G20298.1

Halfar J, Eisele M, Riegl B et al (2012) Modern Rhodolith-dominated carbonates at Punta Chivato, Mexico. Geodiversitas 34:99–113. https://doi.org/10.5252/g2012n1a6

Hammer Ø, Harper DAT (2007) Paleontological data analysis. Blackwell Publishing Ltd.

Hendriks IE, Bouma TJ, Morris EP, Duarte CM (2010) Effects of seagrasses and algae of the Caulerpa family on hydrodynamics and

particle-trapping rates. Mar Biol 157:473–481. https://doi.org/10.1007/s00227-009-1333-8
Hubbard CR, Snyder RL (1988) RIR - measurement and use in quantitative XRD. Powder Diffr 3:74–77. https://doi.org/10.1017/S0885715600013257
Iuppa C, Cavallaro L, Vicinanza D, Foti E (2015) Investigation of suitable sites for wave energy converters around Sicily (Italy). Ocean Sci 11:543–557. https://doi.org/10.5194/os-11-543-2015
James NP, Bone Y, Collins LB, Kyser TK (2001) Surficial sediments of the Great Australian Bight: facies dynamics and oceanography on a vast cool-water carbonate shelf. J Sediment Res 71:549–567. https://doi.org/10.1306/102000710549
Jarochowska E (2012) High-resolution microtaphofacies analysis of a carbonate tidal channel and tidally influenced lagoon, Pigeon Creek, San Salvador island, Bahamas. Palaios 27:151–170. https://doi.org/10.2110/palo.2011.p11-063r
Jongsma D, van Hinte JE, Woodside JM (1985) Geologic structure and neotectonics of the North African Continental Margin south of Sicily. Mar Pet Geol 2:156–179. https://doi.org/10.1016/0264-8172(85)90005-4
Kiessling W, Flügel E, Golonka J (1999) Paleoreef maps: Evaluation of a comprehensive database on phanerozoic reefs. Am Assoc Pet Geol Bull 10:1552–1587
Kiessling W, Flügel E, Golonka J (2002) Phanerozoic reef patterns. SEPM Spacial Publication
Lanfranco E, Rizzo M, Hall-Spencer J et al (1999) Maerl-forming coralline algae and associated phytobenthos from the Maltese Islands. Cent Mediterr Nat 3:1–6
Larkum AWD, Drew EA, Crossett RN (1967) The vertical distribution of attached Marine Algae in Malta. J Ecol 55:361. https://doi.org/10.2307/2257881
Laugié M, Michel J, Pohl A et al (2019) Global distribution of modern shallow-water marine carbonate factories: a spatial model based on environmental parameters. Sci Rep 9:16432. https://doi.org/10.1038/s41598-019-52821-2
Lentz SJ, Fewings MR (2012) The wind- and wave-driven inner-shelf circulation. Ann Rev Mar Sci 4:317–343. https://doi.org/10.1146/annurev-marine-120709-142745
Leukart P, Lüning K (1994) Minimum spectral light requirements and maximum light levels for long-term germling growth of several red algae from different water depths and a green alga. Eur J Phycol 29:103–112. https://doi.org/10.1080/09670269400650551
Linke P, Schmidt M, Rohleder M et al (2015) Novel online digital video and high-speed data broadcasting via standard coaxial cable onboard marine operating vessels. Mar Technol Soc J 49:7–18. https://doi.org/10.4031/MTSJ.49.1.2
Lokier SW, Al Junaibi M (2016) The petrographic description of carbonate facies: are we all speaking the same language? Sedimentology 63:1843–1885. https://doi.org/10.1111/sed.12293
Mariani L, Coletti G, Mateu-Vicens G et al (2022) Testing an indirect palaeo-seagrass indicator: Benthic foraminifera from the Lower Pleistocene Posidonia meadow of Fauglia (Tuscany, Italy). Mar Micropaleontol 173:102126. https://doi.org/10.1016/j.marmicro.2022.102126
Martin S, Gattuso J-P (2009) Response of Mediterranean coralline algae to ocean acidification and elevated temperature. Glob Chang Biol 15:2089–2100. https://doi.org/10.1111/j.1365-2486.2009.01874.x
Mateu-Vicens G, Brandano M, Gaglianone G, Baldassarre A (2012) Seagrass-meadow sedimentary facies in a mixed siliciclastic-carbonate temperate system in the Tyrrhenian Sea (Pontinian Islands, Western Mediterranean). J Sediment Res 82:451–463. https://doi.org/10.2110/jsr.2012.42
Micallef A, Le Bas TP, Huvenne VAI et al (2012) A multi-method approach for benthic habitat mapping of shallow coastal areas with high-resolution multibeam data. Cont Shelf Res 39–40:14–26. https://doi.org/10.1016/j.csr.2012.03.008
Micallef A, Georgiopoulou A, Mountjoy J et al (2016) Outer shelf seafloor geomorphology along a carbonate escarpment: The eastern Malta Plateau, Mediterranean Sea. Cont Shelf Res 131:12–27. https://doi.org/10.1016/j.csr.2016.11.002
Micallef A, Georgiopoulou A, Bas T Le, et al (2013) Processes on the precipice : seafloor dynamics across the upper Malta-Sicily escarpment. In: Rapport Commission Internationale Mer Méditerranée. Commission Internationale pour l'Exploration Scientifique de la Mer Mediterranee, pp 39–40
Michel J, Laugié M, Pohl A et al (2019) Marine carbonate factories: a global model of carbonate platform distribution. Int J Earth Sci 108:1773–1792. https://doi.org/10.1007/s00531-019-01742-6
Mitch (Mitch) PM, Purkis SJ, Ellis J et al (2015) Mapping bathymetry and depositional facies on Great Bahama Bank. Sedimentology 62:566–589. https://doi.org/10.1111/sed.12159
Nalin R, Basso D, Massari F (2006) Pleistocene coralline algal buildups (corallige `ne de plateau) and associated bioclastic deposits in the sedimentary cover of Cutro marine terrace (Calabria, southern Italy). Cool Carbonates Depos Syst Palaeoenviron Control. https://doi.org/10.1144/GSL.SP.2006.255.01.02
Nebelsick JH, Bassi D (2000) Diversity, growth forms and taphonomy: key factors controlling the fabric of coralline algae dominated shelf carbonates. Geol Soc London, Spec Publ 178:89–107. https://doi.org/10.1144/GSL.SP.2000.178.01.07
Osler JC, Algan O (1999) A high resolution seismic sequence analysis of the Malta Plateau
Pedley MH, Carannante G (2006) Cool-water carbonates: depositional systems and palaeoenvironmental controls. Geol Soc London Spec Publ 255:373. https://doi.org/10.1144/GSL.SP.2006.255.01.21
Pérès J-M, Picard J (1964) Nouveau manuel de bionomie benthique de la mer Méditerranée. Stn Mar d'Endoume 31:5–137
Perrin C, Bosellini FR (2012) Paleobiogeography of scleractinian reef corals: changing patterns during the Oligocene-Miocene climatic transition in the Mediterranean. Earth-Science Rev 111:1–24. https://doi.org/10.1016/j.earscirev.2011.12.007
Placenti F, Schroeder K, Bonanno A et al (2013) Water masses and nutrient distribution in the Gulf of Syrte and between Sicily and Libya. J Mar Syst 121–122:36–46. https://doi.org/10.1016/j.jmarsys.2013.03.012
Pomar L (2001) Types of carbonate platforms: a genetic approach. Basin Res 13:313–334. https://doi.org/10.1046/j.0950-091X.2001.00152.x
Pomar L, Baceta JI, Hallock P et al (2017) Reef building and carbonate production modes in the west-central Tethys during the Cenozoic. Mar Pet Geol 83:261–304. https://doi.org/10.1016/j.marpetgeo.2017.03.015
Pomar L, Kendall CGSC (2008) Architecture of carbonate platforms: a response to hydrodynamics and evolving ecology. In: Lukasik J, Simo JA (eds) Controls on carbonate platform and reef development. SEPM Spacial Publication 89, pp 187–216
Prampolini M, Foglini F, Biolchi S et al (2017) Geomorphological mapping of terrestrial and marine areas, northern Malta and Comino (central Mediterranean Sea). J Maps 13:457–469. https://doi.org/10.1080/17445647.2017.1327507
Prampolini M, Blondel P, Foglini F, Madricardo F (2018) Habitat mapping of the Maltese continental shelf using acoustic textures and bathymetric analyses. Estuar Coast Shelf Sci 207:483–498. https://doi.org/10.1016/j.ecss.2017.06.002
Rasband W, Contributors (2021) ImageJ 1.53e
Rasser MW (2000) Coralline red algal limestones of the late Eocene alpine Foreland Basin in Upper Austria: component analysis, facies and palecology. Facies 42:59–92. https://doi.org/10.1007/BF02562567

Reich S, Di Martino E, Todd JA et al (2015) Indirect paleo-seagrass indicators (IPSIs): a review. Earth-Science Rev 143:161–186. https://doi.org/10.1016/j.earscirev.2015.01.009

Reijmer JJG (2021) Marine carbonate factories: review and update. Sedimentology 68:1729–1796. https://doi.org/10.1111/sed.12878

Reijmer JJG, Swart PK, Bauch T, et al (2009) A Re-evaluation of facies on great Bahama bank I: New facies maps of western great Bahama bank. In: Swart PK, Eberli GP, McKenzie JA, et al. (eds) Perspectives in carbonate geology. Wiley, pp 29–46

Reolid J, Bialik OM, Lindhorst S et al (2024) A new type of Halimeda bioherm on the Queensland Plateau NE Australia. Coral Reefs. https://doi.org/10.1007/s00338-024-02500-0

Reuther C-D, Ben-Avraham Z, Grasso M (1993) Origin and role of major strike-slip transfers during plate collision in the central Mediterranean. Terra Nov 5:249–257. https://doi.org/10.1111/j.1365-3121.1993.tb00256.x

Rilov G (2016) Multi-species collapses at the warm edge of a warming sea. Sci Rep 6:36897. https://doi.org/10.1038/srep36897

Rindi F, Braga JC, Martin S et al (2019) Coralline Algae in a Changing Mediterranean Sea: how can we predict their future, if we do not know their present? Front Mar Sci. https://doi.org/10.3389/fmars.2019.00723

Sañé E, Ingrassia M, Chiocci FL et al (2021) Characterization of rhodolith beds-related backscatter facies from the western Pontine Archipelago (Mediterranean Sea). Mar Environ Res 169:105339. https://doi.org/10.1016/j.marenvres.2021.105339

Savini A, Basso D, Alice Bracchi V et al (2012) Maerl-bed mapping and carbonate quantification on submerged terraces offshore the Cilento peninsula (Tyrrhenian Sea, Italy). Geodiversitas 34:77–98. https://doi.org/10.5252/g2012n1a5

Schlager W (2003) Benthic carbonate factories of the Phanerozoic. Int J Earth Sci 92:445–464. https://doi.org/10.1007/s00531-003-0327-x

Schlager W (2005) Carbonate sedimentology and sequence stratigraphy. SEPM (Society for Sedimentary Geology), Oklahoma

Schmitt D, Gischler E (2017) Recent sedimentary facies of Roatan (Bay Islands, Honduras), a Caribbean oceanic barrier reef system. Facies 63:5. https://doi.org/10.1007/s10347-016-0485-5

Sciberras M, Rizzo M, Mifsud JR et al (2009) Habitat structure and biological characteristics of a maerl bed off the northeastern coast of the Maltese Islands (central Mediterranean). Mar Biodivers 39:251–264. https://doi.org/10.1007/s12526-009-0017-4

Smith TB, Frankel E, Jell JS (1998) Lagoonal sedimentation and reef development on Heron Reef, southern Great Barrier Reef province. In: Reefs and Carbonate Platforms in the Pacific and Indian Oceans. pp 281–294

Suarez R, Cook G et al (2019) Sea surface circulation structures in the Malta-Sicily channel from remote sensing data. Water 11:1589. https://doi.org/10.3390/w11081589

Sutton T, Dassau O, QGIS Team (2021) QGIS 3.16

Telesca L, Belluscio A, Criscoli A et al (2015) Seagrass meadows (Posidonia oceanica) distribution and trajectories of change. Sci Rep 5:12505. https://doi.org/10.1038/srep12505

Testa V, Bosence DWJ (1999) Physical and biological controls on the formation of carbonate and siliciclastic bedforms on the northeast Brazilian shelf. Sedimentology 46:279–301. https://doi.org/10.1046/j.1365-3091.1999.00213.x

Tucker ME, Wright VP (1990) Carbonate sedimentology. Blackwell Publishing Ltd., Oxford, UK

UNESCO (1981) Tenth report of the joint panel on oceanographic tables and standards. Unesco technical papers in marine science 36

Vacchi M, De Falco G, Simeone S et al (2017) Biogeomorphology of the Mediterranean *Posidonia oceanica* seagrass meadows. Earth Surf Process Landforms 42:42–54. https://doi.org/10.1002/esp.3932

Vale NF, Amado-Filho GM, Braga JC et al (2018) Structure and composition of rhodoliths from the Amazon River mouth, Brazil. J South Am Earth Sci 84:149–159. https://doi.org/10.1016/j.jsames.2018.03.014

Vallis GK (2017) Atmospheric and oceanic fluid dynamics - fundamentals and large-scale circulation. Cambridge University Press, Cambridge, UK

Villas-Bôas AB, Tâmega FTDS, Andrade M et al (2014) Experimental effects of sediment burial and light attenuation on two coralline algae of a deep water Rhodolith Bed in Rio de Janeiro, Brazil. Cryptogam Algol 35:67–76. https://doi.org/10.7872/crya.v35.iss1.2014.67

Vizzini S (2009) Analysis of the trophic role of Mediterranean seagrasses in marine coastal ecosystems: a review. Bot Mar 52:383–393. https://doi.org/10.1515/BOT.2009.056

Warn-Varnas A, Sellschopp J, Haley P et al (1999) Strait of Sicily water masses. Dyn Atmos Ocean 29:437–469. https://doi.org/10.1016/S0377-0265(99)00014-7

Westphal H, Halfar J, Freiwald A (2010) Heterozoan carbonates in subtropical to tropical settings in the present and past. Int J Earth Sci 99:153–169. https://doi.org/10.1007/s00531-010-0563-9

Williams HD, Burgess PM, Wright VP et al (2011) Investigating carbonate platform types: multiple controls and a continuum of geometries. J Sediment Res 81:18–37. https://doi.org/10.2110/jsr.2011.6